Global molecular landscape of early MASLD progression in obesity

Qing Zhao[1,2,3*], William De Nardo[4*], Ruoyu Wang[5,10*], Yi Zhong[8], Umur Keles[10], Gabrielé Sakalauskaite[10], Li Na Zhao[10], Huiyi Tay[1,2], Sonia Youhanna[8], Mengchao Yan[9], Ye Xie[9], Youngrae Kim[1,2], Sungdong Lee[1,2], Rachel Liyu Lim[1,2], Guoshou Teo[1,2], Pradeep Narayanaswamy[7], Paul R. Burton[6], Volker M. Lauschke[8,9], Hyungwon Choi[1,2,3#], Matthew J. Watt[4,#], and Philipp Kaldis[10,#,&]

[1]Department of Medicine, Yong Loo Lin School of Medicine, National University of Singapore, Singapore
[2]Singapore Lipidomics Incubator, Life Sciences Institute, National University of Singapore, Singapore
[3]Cardiovascular & Metabolic Disease Translational Research Programme, Yong Loo Lin School of Medicine, National University of Singapore, Singapore
[4]Department of Anatomy and Physiology, School of Biomedical Sciences, Faculty of Medicine Dentistry and Health Sciences, University of Melbourne, Melbourne, Victoria, Australia
[5]Department of Hepatology, The First Hospital of Hunan University of Chinese Medicine, Changsha, Hunan, China
[6]Department of Surgery, School of Translational Medicine, Monash University, Melbourne, Victoria, 3004, Australia and Bariatric Unit, Department of General Surgery, The Alfred Hospital, Melbourne, Victoria, 3004, Australia
[7]SCIEX, R&D, Singapore
[8]Department of Physiology and Pharmacology and Centre of Molecular Medicine, Karolinska Institutet, 171 77 Stockholm, Sweden
[9]Dr. Margarete Fischer-Bosch Institute of Clinical Pharmacology, Stuttgart, Germany.
[10]Department of Clinical Sciences Malmö and Lund University Diabetes Centre (LUDC), Lund University, Clinical Research Centre (CRC), 202 13 Malmö, Sweden

[#]Correspondence should be addressed to PK (phone +4673 776 8101; philipp.kaldis@med.lu.se), MJW (matt.watt@unimelb.edu.au) or HC (hyung_won_choi@nus.edu.sg) – [&]Lead Contact

Running title: Dual-omics in obese individuals with MASLD

Keywords: Metabolic dysfunction-associated steatotic liver disease; Lipid metabolism; Fibrosis; GTPase signaling; Obesity

Summary

Metabolic dysfunction-associated steatotic liver disease (MASLD) is often asymptomatic early on but can progress to irreversible conditions like cirrhosis. Due to limited access to human liver biopsies, systematic and integrative molecular resources remain scarce. In this study, we performed transcriptomic analyses on liver and metabolomic analyses on liver and plasma samples from morbidly obese individuals without liver pathology or at early-stage MASLD. While, the plasma metabolomic profile did not fully mirror liver histological features, dual-omics integration of liver samples revealed significantly remodeled lipid and amino acid metabolism pathways. Integrative network analysis uncoupled metabolic remodeling and gene expression as independent features of hepatic steatosis and fibrosis progression, respectively. Notably, GTPases and their regulators emerged as a novel class of genes linked to early liver fibrosis. This study offers a detailed molecular landscape of early MASLD in obesity and highlights potential targets of obesity-linked liver fibrosis.

Introduction

Metabolic dysfunction-associated steatotic liver disease (MASLD) is the most common chronic liver disease, affecting over 30% of adults worldwide [1]. The prevalence of MASLD is closely associated with the epidemic of obesity, with an estimated 75% prevalence among individuals with obesity compared to 32% in the general population [2]. As liver manifestation of the metabolic syndrome, MASLD can cause, and is also caused by concurrent metabolic abnormalities commonly seen in obese individuals, such as insulin resistance, diabetes, dyslipidemia, and hypertension [3, 4].

Early stages of MASLD are characterized by hepatic steatosis, which is the excessive deposition of triacylglycerol (TAG) rich lipid droplets (LD) within the liver parenchyma and is usually reversible. However, in a subset of patients, the disease can develop into inflammatory and ballooning stages termed metabolic dysfunction-associated steatohepatitis (MASH), a more severe form of the disease with an increased incidence and severity of fibrosis. Fibrosis can be present at any stage of the MASLD spectrum of disease and at each stage is increasingly associated with treatment complications, liver-related and overall mortality [5-7]. Unresolved fibrosis can progress to end-stage diseases including hepatic cirrhosis, and hepatocellular carcinoma, lethal malignancies with limited treatment options [8, 9].

Metabolic dysfunction is a primary feature and contributor of MASLD pathogenesis [10]. Hepatic steatosis is often accompanied by increased glucose production [11], elevated de novo lipogenesis [12], and disrupted cholesterol homeostasis [13]. Mitochondrial respiration is adaptively upregulated to prevent lipid accumulation in obesity [14], but with MASLD progression, mitochondria can become dysfunctional and exacerbate metabolic dysregulation [15]. These interconnected metabolic phenotypes form the basis for the development of MASLD [16, 17]. Recent advancements in metabolomics have greatly enhanced the understanding of the molecular systems biology of MASLD [18, 19], however, few studies have combined such analysis with transcriptomics to provide integrative insights into disease pathogenesis in humans.

<u>Fibrosis is the only histological feature of MASLD</u> associated with liver-related mortality and morbidity [20]. In the injured liver, damaged and apoptotic hepatocytes modulate the crosstalk between hepatocytes, liver macrophages (Kupffer cells), and hepatic stellate cells (HSCs) by releasing fibrogenic cytokines (e.g., TGF-β) and activating multiple signaling pathways [21, 22]. As a result of the multicellular response, HSCs transdifferentiate into active, collagen-producing myofibroblasts, driving fibrogenesis and the excessive deposition of extracellular matrix (ECM) [22]. Since fibrosis is a key prognostic marker of MASLD progression, the shift from steatosis to fibrosis marks a critical point in the disease, offering a key opportunity for intervention to prevent further progression [23]. Despite the availability of certain guidelines for clinical management of MASLD [24, 25], the molecular and metabolic changes underpinning the key transitions driving disease progression in the context of obesity remain poorly understood. This poses a challenge to early disease management and prevention.

In this study, we generated a comprehensive map of gene expression and metabolomic profiles to delineate the molecular events associated with early-stage MASLD progression in obesity. Using this multi-omic resource, we focused our investigation on key molecular changes associated with (a) the transition from obesity with normal hepatic histology to MASLD and (b) the onset of liver fibrosis. Our data reveal distinct molecular signatures underlying steatosis and fibrosis

progression, offering a detailed molecular portrait of the liver in early MASLD and highlighting potential therapeutic targets for reversing fibrosis at initial stages.

Results

Overview of the study

We analyzed samples from 109 obese individuals recruited before bariatric surgery at The Avenue, Cabrini, or Alfred Hospitals in Melbourne, Australia (**Table 1** and **Table S1**). Following the exclusion criteria described in Materials and Methods, 33 individuals lacked histological abnormalities (no MASLD) and 76 had MASLD (**Figure 1A**). Notably, 83 individuals (76%) were females in this cohort. Most individuals with obesity were in the early disease stages, with 74 individuals (68%) displaying grade 0-1 steatosis and 83 (76%) grade 0-1 fibrosis. Hepatic inflammation and ballooning were mild, with 9 cases exhibiting grade 2 or higher inflammation and only one case showing grade 2 ballooning (**Figure 1B** and **Table 1**). In clinical tests, MASLD patients displayed worse liver function (higher alanine transaminase (ALT)/aspartate aminotransferase (AST) ratio and gamma-glutamyl transpeptidase (GGT) levels), higher non-high-density (HDL) lipoprotein cholesterol and blood triglyceride levels, higher C-peptide, and insulin resistance compared to those with 'No MASLD' (**Table 1**, $p < 0.05$), confirming correct classification. Liver fibrosis was strongly correlated with insulin resistance, while steatosis grades were most correlated with the levels of plasma lipids (**Figure 1C**).

We performed parallel transcriptomic profiling of liver slices and metabolomic analysis of liver and plasma samples (see Materials and Methods). Untargeted metabolomics (covering polar & non-polar metabolites including lipids) enabled semi-quantification of 1104 liver and 962 plasma metabolites, respectively (**Figure 1D**). Plasma urea and creatinine levels from untargeted metabolomics closely correlated with clinical assays (**Figure S1A**), supporting data reliability. Principal component analysis (PCA) revealed distinct clustering of the liver metabolome by MASLD status, but not in plasma (**Figure 1E**). The liver transcriptome was modestly separated between individuals with and without MASLD along the main principal components (**Figure 1F**), indicating that transcriptional programs may be shaped by both MASLD histological progression and confounding metabolic and biological processes in obese individuals (**Table S2**).

As steatosis and fibrosis are the key histological features of MASLD, our statistical analyses focused on identifying molecular determinants linearly associated with their progression (**Table S3-5**). Models were adjusted for patient characteristics (age, sex, and BMI) and type 2 diabetes, the latter due to its differing prevalence across disease groups (**Table 1**). Moreover, we compared our transcriptomic data with those from two additional published cohorts: the Virginia cohort (VA cohort, GSE130970) [26] with a disease spectrum comparable to that of our study, and the European cohort (EU cohort, GSE135251) [27, 28] with a broader spectrum of the disease covering advanced MASLD pathologies (**Figure 1G**).

Global investigation of the metabolome in obese MASLD patients

As expected, the liver metabolome was extensively remodeled in individuals with MASLD. Steatosis is the primary histological feature linked to liver metabolome, with 206 metabolites showing significant positive associations and 242 showing negative associations ($q < 0.05$, **Figure 2A** and **Figure S1B**). For example, we observed higher levels of glycerolipids (GLs, e.g. TAGs, diacylglycerols [DAGs]) and lower levels of membrane lipid classes, especially glycerophospholipids (GPLs) (**Figure**

2A-B and **Figure S1B**). Specifically, TAGs with 0 to 5 double bonds in the fatty acyl chains were positively associated with the histological outcomes, whereas TAGs containing at least one polyunsaturated fatty acid (PUFA) chain (e.g. number of double bonds > 5) were negatively associated with disease progression, particularly with steatosis **(Figure S1C**). Our findings are likely the results of increased de novo lipogenesis and elevated hepatotoxicity associated with saturated fatty acids [29, 30].

The plasma metabolome displayed limited associations with the histological features (**Figure 2A**), with statistically significant associations primarily with steatosis, such as TAGs (q value < 0.05, n = 22) and ether-linked TAG (TAG-O, q value < 0.05, n = 8) species. To better interpret the plasma metabolome data, we performed partial correlation network analysis to assess the associations among circulating metabolites, clinical variables, and hepatic histology in individuals with obesity [31]. The network demonstrates the highest connectivity of plasma metabolites with clinical variables and fewer connections with hepatic histology features (**Figure 2C**). This implies that plasma metabolome largely reflects other metabolic conditions such as kidney function, dyslipidemia, and insulin resistance rather than hepatic features. Most plasma lipid classes were correlated with blood lipoprotein cholesterol levels (**Figure 2D**). However, in the context of obesity, blood lipoprotein levels did not show strong correlation with MASLD progression (**Figure S2**), indicating that their broad impact on plasma metabolome may mask the signals from hepatic abnormalities.

We next compared steatosis- and fibrosis-associated metabolite changes in the liver and plasma (**Figure 2E**). Plasma GLs exhibited similar but weaker associations with liver steatosis compared to hepatic GLs, whereas the depletion of PUFA-containing TAGs in the liver was not mirrored in circulation. Although plasma polar metabolites showed changes in the context of steatosis, potential circulating markers emerged for liver fibrosis with mild statistical significance. With fibrosis progression, there was a trend toward increased levels of tyrosine, quinolinic acid, lactic acid, and kynurenic acid in plasma ($p < 0.05$, $q > 0.05$) (**Table S3**), consistent with their reported roles as key hepatic metabolites implicated in MASLD progression and as proposed circulating biomarkers for MASLD severity or biopsy-proven MASH [32-35]. Overall, despite elevated TAG levels and potential fibrosis indicators, the circulating metabolome is less indicative of early-stage MASLD-related alterations in individuals with obesity and obesity-related co-morbidities.

Integrative view of liver metabolism remodeling

We next integrated the hepatic metabolome and transcriptome to characterize metabolic remodeling in obese individuals during early disease development.

Lipid metabolism

In the liver, accumulation of GLs and mild reduction of GPLs were the main features of the metabolome changes (see **Figure 2**). Consistent with this observation, we identified genes implicated in the homeostasis of GLs and GPLs (**Figure 3A** and **Figure S3**). Genes such as *DGAT2*, *PNPLA3*, and *PLIN3* play a role in LD formation and TAG and DAG metabolism [36]. GPL metabolism was also markedly altered, including key genes such as *LPCAT1*, *PLD2*, *PCYT2*, *ETNK*2 and that are implicated in a compensatory response to the shift in phospholipid metabolism and the increased turnover of GPLs [37, 38]. In individuals with advanced hepatic fibrosis, expression levels of the genes involved in primary bile acid biosynthesis, such as *SLC27A5, AMACR*, *ACOX2*, *AKR1C4*, and *BAAT*, were lower. In addition, a group of

cytochrome P450 (CYP) genes were downregulated during the progression of fibrosis, particularly those involved in CYP-dependent PUFA metabolism (i.e., linoleic acids and arachidonic acids into bioactive molecules) and steroid hormone biosynthesis [39, 40] (**Figure 3A**). Overall, our data highlights a number of genes encoding the enzyme subunits of anabolic and catabolic lipid metabolism in early MASLD, and some of these gene signals were consistently observed in both the EU and VA cohorts [26, 27].

Dysregulated metabolic pathways during steatosis progression

To explore the variation in metabolic activities using dual-omic descriptors, we prioritized key pathways with both dysregulated metabolites and gene expressions (**Figure 3B**). In addition to significant GL and GPL remodeling, we also identified altered pathways of amino acid metabolism at both omics levels. Elevated levels of amino acids including glycine, glutamic acid, arginine, serine, and alanine in steatotic livers may reflect increased collagen synthesis and ECM remodeling during MASLD progression [41, 42] (**Figure 3C-D**). Notably, aromatic amino acids including phenylalanine, tyrosine, and tryptophan were lower in subjects with advanced steatosis (**Figure 3D**). Dual-omics data revealed consistent downregulation of tryptophan metabolism, encompassing both the indole and melatonin pathways (**Figure 3C**). However, quinolinic acid, a key metabolite in the kynurenine pathway and a product of tryptophan catabolism, was significantly elevated in association with both hepatic steatosis and fibrosis. Collectively, early MASLD development is associated with reduced aromatic amino acid levels and the altered tryptophan catabolic flux in the liver, potentially reflecting the aberrant gut–liver axis communication in obese MASLD patients [43-45].

Moreover, homocysteine and its upstream metabolite S-adenosylhomocysteine levels were significantly higher in steatotic livers, indicating dysregulated methylation with excessive lipid storage [46]. However, the accumulation these metabolites was mitigated by fibrosis-associated downregulation in key enzymes including *GNMT*, *MAT1A*, and *AHCY* (**Figure 3C**), which have been linked to liver pathogenesis in in vivo models [47-50]. These suggest that an imbalance in methylation reactions of DNA and proteins may be an important mediator of liver fibrogenesis in obese individuals.

In addition, we observed elevated levels of the antioxidant coenzyme Q10 (CoQ10; ubiquinone) and its intermediates CoQ6 and CoQ9 in the steatotic liver (**Figure 3D**). Higher levels of two other antioxidants, taurine and alpha-tocopherol (vitamin E), were also detected. Another indicator of oxidative stress, hydroxybutyric acid, was increased in advanced steatosis and is also recognized as an early marker of insulin resistance [51]. Overall, the progression of liver steatosis is accompanied by extensive changes in amino acid metabolism and oxidative stress regulation.

Dysregulated genes involved in mitochondrial function and autophagy

In the liver metabolome, lower levels of hepatic long-chain acyl-carnitine (CAR) species were observed with advanced steatosis (CAR 18:2 and 20:4**, Table S4**), suggesting dysregulated fatty acid transmembrane transport and β-oxidation [52, 53]. To systematically assess mitochondrial functions beyond β-oxidation, we mapped steatosis and fibrosis-associated genes to MitoCarta3.0 [54]. Distinct mitochondrial dysfunction patterns emerged: steatosis involved 26 downregulated and 55 upregulated mitochondrial-function genes, including 16 related to mtDNA maintenance, while fibrosis was linked to 151 downregulated (dark green) and only

15 upregulated (orange) genes (**Figure 4A** and **Table S6**). These transcriptional shifts suggest that hepatic fibrosis involves broad mitochondrial impairment, contributing to oxidative stress and reduced ATP production, which could favor the exacerbation of steatohepatitis [15].

Autophagy serves as a critical cellular response mechanism to the overload of intrahepatic TAG and cholesterol [55, 56]. Metabolomic analysis showed increased free cholesterol and reduced levels of CE 18:1 and 18:2, the predominant hepatic CE species [57] (**Figure S4A**), supporting prior findings that CE de-esterification contributes to elevated free cholesterol in MASLD [58]. Although autophagy has been linked to HSC activation [59, 60], its involvement in MASLD progression remains unclear. Using a list of predictive genes in autophagy activation [61], we found that autophagy activation and lysosome biogenesis were more strongly associated with steatosis than fibrosis, with upregulated key autophagy genes such as *ULK1* and *MTOR* (**Figure 4B**). Further investigation of over 600 autophagy genes [61] (**Table S7** and **Figure S4B**) revealed active autophagy initiation in early MASLD, where 119 genes across pathways including mTORC and upstream effectors, lysosome, and autophagy core assembly genes displayed altered expression levels. This suggests that autophagy serves as an adaptive response to hepatic lipotoxicity during steatosis, but its activation may decline as the disease progresses, as evidenced by the downregulation of key regulators such as *NR1H4*, *SIRT5*, *FOS*, and *EGR1* (**Figure S4B**), thereby impairing liver metabolism [62].

Molecular signatures of hepatic steatosis and fibrosis are mutually independent

To gain insights into the dual-omic data in the liver further, we performed a partial-correlation network analysis to integrate liver transcriptomic, metabolomic, and clinical data [31]. The resulting subnetwork highlighted distinct molecular signatures correlated with steatosis and fibrosis (**Figure 5A**). Steatosis was primarily associated with hepatic neutral lipid accumulation and related metabolomic alterations, whereas fibrosis was predominantly linked to transcriptional changes, including the upregulation of genes involved in ECM remodeling (e.g., *TGFB3*, *FSTL1*), signal transduction (e.g., *RHOU*, *DOK3*), and metabolism (e.g., *CYP2C19*, *PNPLA4*, *SGPL1*). These findings underscore the presence of distinct molecular pathways driving the progression of steatosis and fibrosis.

In our transcriptomics analysis, 992 and 1,251 gene markers were identified as significantly associated with the histological features of steatosis and fibrosis, respectively, with limited overlap between the two sets (**Figure 5B** and **Table S5**, q value < 0.05), suggesting unique transcriptomic regulations underlie each feature. Functional enrichment analysis further supported this distinction, revealing largely non-overlapping biological processes associated with each gene set (**Figure S5** and **Table S8**).

To distinguish gene signatures uniquely linked to steatosis or fibrosis, we included the other histological feature as a covariate in the regression model. This allowed us to define steatosis-specific genes (independent of fibrosis) and fibrosis-specific genes (independent of steatosis) (**Table S9**). Since steatosis precedes fibrosis in the pathophysiology of MASLD, enrichment analysis of steatosis- and fibrosis-specific genes revealed a 'pseudo-temporal' progression of biological processes (**Figure 5C**). More pathways were found to be associated with fibrosis than with steatosis. Steatosis-specific upregulated genes were enriched in protein glycosylation, inflammatory response, lipid catabolism, and lysosome organization.

In contrast, fibrosis-specific genes showed downregulation of various metabolic pathways and upregulation of processes related to ECM remodeling, hypoxia, signaling, and cell morphogenesis. Additionally, apoptosis-related pathways were suppressed in steatosis but activated in fibrosis, while nucleotide metabolism showed the opposite trend, suggesting dynamic regulation of cell death and proliferation during MASLD development. These findings implicate distinct and lesion-specific gene regulatory programs in early MASLD progression.

Moreover, consistent with previous observations showing that hepatic fibrosis correlates with insulin resistance parameters in clinical assays (**Figure 1C**), we found that individuals with diabetic MASLD exhibited a greater number of downregulated genes as fibrosis progressed than non-diabetic MASLD individuals (**Table S10**). Since most of the suppressed genes in the diabetic subgroup are involved in metabolism (e.g., *BAAT*, *G6PC1*, *SULT2A1*, *MAT1A*), we hypothesize that diabetes may exacerbate the metabolic dysfunction associated with hepatic fibrosis progression.

Gene signatures of fibrosis initiation

To further explore representative gene signatures in the development of fibrosis, we identified 213 genes as progressive markers by comparisons of gene expression levels against two different baselines (no MASLD and steatosis; details provided in the methods; **Table S11**). Among them, 75 of these markers overlapped with fibrosis-associated genes in the VA cohort and 35 overlapped with the EU cohort (**Figure 6A**) [26], resulting in 130 novel fibrosis markers. Pathway analysis of these fibrosis markers highlighted prominent roles for signal transduction and ECM organization/ disassembly, as expected (**Figure S6A**). To infer the cell type-of-origin for signals from bulk sequencing, we mapped progressive fibrosis markers onto a human liver single-cell atlas [63]. Upregulated genes appeared to reflect changes from different cell types, whereas downregulated markers were predominantly hepatocyte-specific (**Figure 6A**, left panel). This suggests that in the early stages of liver fibrosis development, the transcriptional programs are activated in different cell types, while hepatocyte functions potentially become muted during the process. Meanwhile, we observed fibrosis-associated upregulation of genes involved in TGF-β and SMAD signaling cascades (*TGFB1*, *TGFB3*, and *INHBA*), ECM activators [64-66] (*ITGAV*, *LOXL2*, *THBS1*, *MMP9*, and *MMP14*), regulators (*CDK8*, *CTDSP2*, *HDAC1*, and *HDAC7*), and downstream targets (*TIMP1*, *MMP9*, and *COL5A2*) (**Figure S6B**). This aligns well with previous reports that TGF-β signaling and HSC activation drive fibrosis during MASLD progression [67, 68].

Given that the transition from simple steatosis to the onset of fibrosis marks a critical window for disease management, we compared gene expression profiles between individuals with fibrosis accompanied by steatosis and those with steatosis but without fibrosis (**Table S12**). Notably, the top-enriched pathways in this comparison emerged as GTPase signaling and its regulation, signal transduction, and innate immune response (**Figure 6B**). Moreover, we identified 37 GTPase-related genes displaying significant associations with fibrosis progression (**Figure S7A** and **Table S13**). To explore the potential role of GTPase signaling in fibrosis, we examined an inventory of 251 genes encoding GTPases, GTPase-activating proteins (GAPs), and guanine nucleotide exchange factors (GEFs), analyzing their interactome using the Human Cell Map [69] and a protein-protein interaction network [70, 71].

Among the 6,971 proteins that have been tested for physical interaction or subcellular proximity with GTPase-related genes, 508 of these associated significantly with fibrosis progression in our cohort (**Figure 6C**). The network indicates that GTPases and their regulators interact with a wide range of fibrosis genes, with *ARF3* and *RAC1* being central hubs of the network. Functional enrichment of the core nodes revealed that the GTPase network regulates intracellular transport, actin cytoskeleton organization, exocytosis, and other biological processes during fibrosis progression (**Figure S7B**). Therefore, GTPases and their regulators are co-regulated with fibrosis-related genes encoding their protein interaction partners, supporting the likelihood of a functional link between GTPases and hepatic fibrosis. This is supported by TGF-β genes positively correlated with co-expressed GTPase-related genes (**Figure S7C**), suggesting a potential link between TGF-β signaling and GTPase pathways.

To experimentally validate our findings, the altered expression of GTPase-related genes was explored in an independent system using an established model of 3D liver spheroids in which hepatic cells remain viable and functional for multiple weeks [72-74]. Specifically, we co-cultured primary human hepatocytes with Kupffer and stellate cells isolated from patients with histologically confirmed MASH [75] and examined the overall expression profile of GTPase-regulated genes between our human cohort and the ex vivo system. The expression of GTPases were largely concordant when assessing human patients and the 3D spheroid system (**Figure 6D**). In comparison to the control group, spheroids from MASH patients demonstrated an upregulation of 24 genes encoding GTPases and their regulators (**Figure 6E**). Remarkably, the treatment of liver spheroids with elafibranor, a dual PPARα/δ agonist [76], restored the expression levels of 17 (70%) GTPase-related genes back to the baseline (**Figure 6E**). This independent system further suggests that GTPases may play a role in MASLD pathogenesis and the fibrotic response.

Since HSCs are the main liver cell type responsible for activating fibrosis, we next assessed whether inhibition of GTPase activity in an immortalized HSC cell line, the LX-2 cells, could attenuate markers of fibrogenesis (**Figure S8A**). Selective GTPase inhibitors targeting Rac1 (NSC23766) and Cdc42 (ML141) reduced the mRNA expression of *COL1A1* and *COL1A2*, as well as pro-collagen secretion (**Figure S8**) under basal conditions. TGF-β1 mediated activation induced the expected increase in collagen secretion and gene expression which was attenuated by Rac1 inhibitor (NSC23766) and to a lesser extent by ML141. In addition, examination of previously published transcriptomic data of HSCs isolated from CCL_4-mediated liver fibrosis in mice [77], revealed the upregulation of GTPases comparable to the steatosis-to-fibrosis transition in our human cohort, with a temporal pattern aligning with hepatic collagen deposition (**Figure S9A**). Further, in a human liver organoid model, TGF-β induced increased expression of GTPase-related genes in hepatocytes and HSCs, but not in fibroblasts [78] (**Figure S9B**), suggesting a potential feedforward loop involving the TGF-β/GTPase axis between hepatocytes and HSCs. To investigate intercellular crosstalk in GTPase regulation, we examined key GTPase-related genes in LX-2 cells, hepatocyte monocultures, and spheroid co-cultures (including hepatocytes, HSCs, Kupffer cells). As shown in **Figure S10**, TGF-β1 induced a potential increase in *VAV1* and *DOCK2* consistent in co-cultures, hepatocytes, and LX-2 cells, while *RAC1*, *RAB32*, and *RHOU* showed cell type-specific responses. These findings indicate that multiple hepatic cell types mediate GTPase regulation, underscoring intercellular crosstalk.

Overall, these additional experiments and analyses of datasets identified upregulated GTPase-related genes during fibrosis initiation (**Figure S9C**). However, further in-depth mechanistic studies are needed to validate this association.

Discussion

In this study, we performed a comprehensive omics-based analysis of a cohort of 109 obese individuals with early MASLD. Through integrative dual-omics approaches, we mapped the liver and plasma metabolomes and identified distinct hepatic molecular features associated with steatosis and fibrosis progression. Notably, fibrosis was closely connected to global reprogramming of hepatic gene expression, with GTPase-related genes emerging as possible mediators of fibrosis initiation.

In this obesity cohort, the plasma metabolome showed limited alterations in MASLD, with the exception of elevated circulating TAGs. This contradicts with McGlinchey *et al*., who reported more than 20 differential metabolites in the serum metabolome [19]. Our conjecture is that the discrepancy stems from the different disease spectrum covered in the two studies, as the cohort in the other study included advanced MASLD cases with NAS score ≥ 4 (63.4%). In addition, our study focused exclusively on obese individuals (median BMI > 43.0), substantially higher than the other study. A recent report has highlighted distinct metabolite signatures between obese and lean individuals with MASLD, noting fewer differential metabolites in obese individuals than lean ones [79]. This suggests that plasma lipidome is less reflective of liver pathology in patients with obesity compared to lean individuals. Similarly, a BMI-stratified multivariable model revealed distinct circulating MASLD metabolite signatures across different degrees of obesity, with lean subgroups showing significantly altered circulating lipotoxic intermediates [80]. Therefore, as shown in **Figure 2C**, we hypothesize that co-occurring morbidities in obesity may obscure liver-derived metabolic signals in the plasma, particularly in early-stage MASLD. Given that obese individuals represent the predominant population affected by MASLD, it is reasonable to conclude that whether blood analysis of metabolites attains diagnostic accuracy in identifying disease progression at early stages depends on the disease spectrum covered in a study and remains context-specific. However, the emergence of liquid biopsies, fine needle liver biopsies, and the evaluation of liver-specific extracellular vesicles may open up other minimally invasive diagnostic opportunities [81].

The strength of our study is the characterization of hepatic pathophysiology in relation to steatosis and fibrosis via transcriptome and metabolome-wide variations. Consistent with general expectation, our work highlighted altered hepatic lipid metabolism in human liver tissues of obese patients at both metabolite and gene levels [82-84]. Consistent with the variations in GLs, higher expression levels of *DGAT2*, *PNPLA3*, and *PLIN3* were associated with steatosis progression. The higher expression of *DGAT2*, which encodes a key enzyme catalyzing the last step of de novo TAG synthesis, implies enhanced integration of TAGs into LDs in the endoplasmic reticulum, which presumably alleviates lipid-induced ER stress and evades accumulation of lipotoxic lipids [85]. Upregulation of *PLIN3* was correlated with higher grades of both fibrosis and steatosis. The protein encoded by *PLIN3*, along with other PLIN proteins [86], plays an important role in LD stabilization and the prevention of TAG hydrolysis, thus potentially contributing to hepatic steatosis [87]. In addition, although previous animal studies have reported increased levels of sphingolipids in MASLD models [19, 88], we did not observe this in patients with obesity

at early stages of the disease. Sphingolipid alterations varied across cohorts with differing patient compositions [18, 19, 89], suggesting that sphingolipid metabolism may be dependent on disease stage, obesity status, and exhibit discrepancies between humans and mice.

Beyond lipid metabolism, other metabolic pathways and processes also exhibited dysregulation at the dual-omics level. Specifically, with excessive lipid deposition, we observed higher levels of taurine and vitamin E, both of which have antioxidant effects and likely reflect the hepatic response to oxidative stress [90-92]. Importantly, amino acid metabolism was markedly dysregulated as steatosis progressed, characterized by elevated hepatic levels of serine, arginine, glutamic acid, glycine, and alanine, along with decreased levels of the aromatic amino acids phenylalanine, tryptophan, and tyrosine. A previous *in vitro* study also demonstrated that palmitic acid supplementation disrupted the metabolism of the aromatic amino acids in PH5CH8 and HepG2 cells [93]. As microbiota-derived metabolites, dysregulation in these amino acid may reflect disrupted gut function and may affect the de novo synthesis of nicotinamide adenine dinucleotide in MASLD patients [94]. Moreover, we also observed evidence of autophagy activation concurrent with intrahepatic lipid and cholesterol accumulation, wherein lysosome-associated genes were uniquely associated with steatosis, as shown in **Figure 4B** and highlighted in **Figure 5C** by the enrichment of lysosome organization among steatosis-specific processes. This autophagic response most likely represents a protective mechanism to ameliorate steatosis [95]; however, the downregulation of autophagy regulators during fibrosis development may exacerbate liver metabolic dysfunction.

As liver fibrosis progressed, the expression levels of genes involved in primary bile acid biosynthesis, PUFA metabolism, and steroid hormone biosynthesis were lower, especially *ACADS*, *ACADSB*, and *ACADM* which encode key enzymes in the initial stage of catalyzing fatty acid β-oxidation, and *HADH* and *ACAA1*, which encode enzymes that act in the late stage of β-oxidation [96]. Moreover, mitochondrial-related genes were downregulated with fibrosis progression, particularly those related to the electron transport chain of the mitochondrial inner membrane. This may indicate that pathological oxidative stress and impaired ATP production caused by early mitochondrial dysfunction may aggravate fatty liver inflammation [14], and the augmentation of the inflammatory response may become an important cause of liver fibrosis.

Through univariate hypothesis testing and partial correlation analysis, we revealed distinct molecular signatures correlated with fibrosis and steatosis. Liver fibrosis was associated with gene expression alteration, from which we identified over 200 progressive markers tracking its gradual advancement. Furthermore, GTPase-related genes were dysregulated at the mRNA level with the emergence and progression of fibrosis. Increased expression of GTPase regulators was independently confirmed in 3D primary human liver spheroids, with elafibranor restoring their expression to baseline levels (**Figure 6E**). The downregulated expression of GTPase regulators following elafibranor treatment suggests a potential anti-fibrotic mechanism involving GTPase signaling.

GTPase proteins are categorized into several subfamilies such as Rho-, Ras-, and Arf-GTPase based on their sequence and structure [97]. GAPs and GEFs are the key regulators of GTPase activity that modulate intrinsic GTPase functions and the GTP-bound state [98]. Only a few studies have elucidated the role of GTPases in liver pathology [99-102]. For instance, *Rap1a* was identified as a signaling molecule that suppresses both gluconeogenesis and hepatic steatosis [102]. The Rab23-specific

GAP, *GP73*, has been implicated in triggering non-obese MASLD [101]. Additionally, Rho-GTPase signaling through the ROCK1/AMPK axis regulates de novo lipogenesis during overnutrition [99], while an immune-related GTPase triggers lipophagy and prevents hepatic lipid storage [100]. However, evidence regarding the role of GTPase regulation in human liver is limited, particularly in the context of liver fibrosis initiation and progression, and a thorough mechanistic investigation is warranted to establish causality.

In recent years, dual- and multi-omics strategies have gradually emerged in MASLD research. A proteo-transcriptomic map constructed from the EU cohort's liver RNA sequencing data and circulating proteome identified four promising protein biomarkers [28]. Among these, *AKR1B10* was also identified in our study as a key gene related to lipid metabolism, showing strong associations with both steatosis and fibrosis (**Figure 3A**), which highlights its potential as a biomarker even in the early stages of MASLD. Additionally, we observed mitochondrial dysregulation linked to the progression of liver fibrosis (**Figure 4A**). Consistent with our findings, a multi-omics study in obese individuals with MASLD also revealed mitochondrial dysfunction at the hepatic protein level. The study further emphasized similar mitochondrial disruptions in adipose tissue, suggesting the liver-adipose tissue interaction in obesity-related MASLD [103]. Beyond inter-tissue interactions, Raverdy *et al*. reported the heterogeneity of MASLD molecular signatures in relation to varying degrees of cardiovascular risk and type 2 diabetes [104]. This further highlights the impact of systemic metabolic conditions on MASLD progression. In our analysis of diabetic individuals, we identified more downregulated metabolic genes associated with fibrosis, supporting the notion that insulin resistance may exacerbate metabolic dysregulation and interferes with the disease trajectory.

Overall, our integrative investigation offers one of the most detailed molecular landscapes of early stage MASLD in individuals with obesity, with comprehensive descriptors of the early remodeling of hepatic metabolism associated with initiation of fibrosis in the steatotic liver.

Limitations of the study

This study focused on 109 patients with early-stage MASLD, potentially overlooking molecular changes associated with later disease stages. To address this, we cross-referenced our findings with two external cohorts (EU and VA). Additionally, we identified GTPase-related genes as potential future targets for reversing liver fibrosis. While preliminary validation has been conducted in different systems, further investigation is required to confirm the causal role of specific GTPases in fibrosis initiation especially in HSCs and to elucidate how GTPase signaling contributes to collagen production throughout the progression of MASLD.

Materials and Methods

Ethics statement

Participants provided written and verbal informed consent. The study protocol conforms to the ethical guidelines of the 1975 Declaration of Helsinki and was approved by the University of Melbourne Human Ethics Committee (ethics ID 1851533), The Avenue Hospital Human Research Ethics Committee (Ramsay Health; ethics ID WD00006, HREC reference number 249), the Alfred Hospital Human Research Ethics Committee (ethics ID GO00005), and Cabrini Hospital Human Research Ethics Committees (ethics ID 09-31-08-15). All work on the data

from human samples in Sweden was approved by Etikprövningsmyndigheten (Dnr 2024-07917-01).

Cohort recruitment

A detailed medical history was taken, and metabolic comorbidities were noted including the presence of previously diagnosed hypertension and diabetes assessed by oral glucose tolerance testing. Exclusion criteria included: age <18 years, previous gender reassignment, other causes of chronic liver disease and/or hepatic steatosis including Wilson's disease, α-1-antitrypsin deficiency, viral hepatitis, human immunodeficiency virus, primary biliary cholangitis, autoimmune hepatitis, genetic iron overload, hypo- or hyperthyroidism, coeliac disease, as well as recent (within three months of screening visit) or concomitant use of agents known to cause hepatic steatosis including corticosteroids, amiodarone, methotrexate, tamoxifen, valproic acid and/or high dose oestrogens [105]. Further exclusion criteria included potential for alcohol-induced liver disease, which was assessed through a modified version of the alcohol use disorders identification test (AUDIT) [105, 106]. Following histological assessment, patients with liver slice weighing less than 2mg were excluded from the omics analysis.

Eligible patients with obesity scheduled for primary or secondary sleeve gastrectomy, gastric bypass, or the insertion of a laparoscopic-adjustable band were prospectively enrolled. All patients were fasted for 8-12 h overnight and venous blood was taken before the induction of anaesthesia. Blood was transferred to 2 x K2E Ethylenediaminetetraacetic acid (EDTA), 2 x SST™ II Advance and 1 x FX 5 mg bio-containers for subsequent storage or clinical/biochemical assessments. All blood samples were sent to Melbourne PathologyTM (Victoria, Australia) for standardised measurement of biochemical and metabolic variables, except for one bio-container of EDTA. Standard blood analyses were performed for electrolytes, full blood examination, glucose, glycosylated haemoglobin, insulin, C-peptide, cholesterol, triglycerides, and liver function assessed by ALT, AST, GGT, and alkaline phosphatase (ALP), and screening blood tests for liver disease. The remaining blood within the EDTA tube was spun at 8000 x g for 10 min and the plasma was collected and stored at -80°C for mass spectrometry analyses.

Liver biopsy collection and histological feature assessment

An ~ 1 cm^3 wedge liver biopsy was collected from the left lobe of the liver during surgery. The liver was cut into two portions. One portion was placed in formalin and transported to TissuPath™ (Mount Waverley, Victoria), paraffin embedded and processed for histological analysis. Samples were graded according to the Clinical Research Network NAFLD activity score (NAS) [107] and Kleiner classification of liver fibrosis [108] by a liver pathologist at TissuPath. Patients with no MASLD were defined by steatosis score of 0, regardless of inflammation or fibrosis grade 1. MASL patients were defined by a steatosis score ≥1 with or without lobular inflammation. MASH was defined by the joint presence of steatosis, lobular inflammation, and ballooning [108]. The remaining portion of liver slices was used for bulk RNA sequencing and untargeted metabolomics analysis.

Sample preparation for untargeted metabolomics

For liver tissue biopsies, each sample containing 50 ± 5 mg of tissue was extracted in 0.8 mL 50:50 (v/v) methanol:chloroform [109, 110]. Samples were homogenized for 10 min at 25 Hz with a single 3-mm tungsten carbide bead per tube. Separation of phases was achieved by the addition of 0.4 mL of water followed by vortex-mixing

and centrifugation (2400 g, 15 min, 4 °C). After separation, the upper phase (the metabolite-containing fraction) and the lower phase (the lipid-containing fraction) were transferred into separate tubes and dried using SpeedVac.

For plasma samples, 225 µL of methanol was added to 50 µl plasma, and the mixture was vortexed for 10 sec [111]. Subsequently, 450 µL chloroform was added and the mixture was incubated for 1h in a shaker. To induce phase separation, 187.5 µL water was added and the mixture was centrifuged at 12,000 rcf for 15 min at 4 °C. The upper phase (the metabolite-containing fraction) phase and lower (the lipid-containing fraction) were collected into separate fresh tubes and dried using SpeedVac.

Dry extracts from the organic fraction were resuspended in the mixed solvent of 90:10 isopropanol: acetonitrile. For the aqueous fraction, 90% acetonitrile was used to reconstitute dry extracts. Plasma samples were reconstituted in 1:4 dilution (plasma-to-solvent: 50 µL/200 µL), and the reconstitution volumes for liver biopsy samples were corrected by the weights of liver slices (tissue-to-solvent: 50 mg/1000 µL). After reconstitution, samples were sonicated for 15 min and centrifuged at 12,000 g for 10 min at 4 °C.

Metabolomics data acquisition and processing

A 1 µL aliquot of the extract was subjected to LC-MS analysis using the Sciex TripleTOF 6600 system coupled with the Agilent 1290 HPLC. For polar metabolite analysis, mobile phase A was water with 10 mM ammonium formate and mobile phase B was acetonitrile with 0.1% formic acid. Flow rate was 0.250 ml/min. The LC gradient started at 3% A, increased to 30% A from 1 to 12 min, then to 90% A from 12 to 15 min, remained at 90% until 18.5 min, and returned to 3%, holding until the end of the 24-min run. For lipid analysis, mobile phase A was prepared by 60:40 water: acetonitrile with 10 mM ammonium formate, and mobile phase B was made by 90:10 isopropanol: acetonitrile with 10 mM ammonium formate. Flow rate was 0.250 ml/min and the total run time is 15.80 min. The LC gradient started at 80% A, decreased to 40% A at 2 min, further decreased to 0% from 2 to 12 min, remained at 0% A until 14 min, then returned to 80% A at 14.10 min, and held at 80% A until the end of run. Mass spectrometry settings were as follows: gas1 50 V, gas2 60V, curtain gas 25V, source temperature 500 °C, IonSpray voltage 5500 V. The collision energy was set to 30 V and 45 V for polar metabolites and lipids, respectively. Fifteen precursors were selected for MSMS fragmentation in the DDA acquisition. The mass range for the RP method was 300 – 1000 m/z and for the HILIC method was 50 – 1000 m/z. In the SWATH acquisition, fixed windows were applied with window widths of 21 Da for the HILIC method and 10 Da for the RP method.

Each tissue type (i.e., plasma and liver) was analyzed as a separate batch. Following sample reconstitution, the supernatants were collected into MS vials and pooled as quality control (QC) samples for each tissue type. For each analytical batch, patient samples were injected in a randomized sequence, along with one QC injection approximately every 10 samples for monitoring instrument stability and calculating the coefficient of variation (CoV). Both reverse phase (RP) and hydrophilic interaction liquid chromatography (HILIC) columns were used for chromatographic separations of organic and aqueous fractions, respectively. For the analysis of aqueous fraction, metabolites were separated on SeQuant ZIC-cHILIC (3 µm, 100Å, 100x2.1 PEEK) column with a flow rate of 0.25 mL/min in a 24-minute run. For the organic fraction, metabolites were separated on RRHD Eclipse Plus C18 (2.1 x 50 mm, 1.8 µm).

Data acquisition was performed in both positive and negative ionization modes. Data-dependent acquisition (DDA) was performed on pooled QC samples for compound identification and SWATH-MS analysis was applied to individual samples for relative quantification. The mass range for the RP method was 300 – 1000 m/z and for the HILIC method was 50 – 1000 m/z. Data was converted into mzML format and was then processed by MetaboKit [112] (https://github.com/MetaboKit). To gain broad metabolite coverage, we curated a data processing pipeline for metabolites identified via spectral matches (MSMS-level, with 915 identifications postprocessing) and those identified solely through mass matches (MS1-level, with 548 identifications postprocessing). For metabolite quantification, the project-specific spectral library generated from DDA analysis was used to extract MS1 and MS2 features from the SWATH data using the MetaboKit DIA module. Compound transitions with a CoV > 30% were excluded from the analysis. For each compound, the precursor or fragment ion with the lowest CoV was selected as the quantifier. For a compound identified in both positive and negative modes using the same column, the peak feature with the lower CoV were selected. Overlapping metabolites in the RP and HILIC datasets are mainly semi-polar lipids, as RP detects compounds with m/z > 300. For lipids identified by both methods, the ones measured on the RP column was selected.

RNA sequencing

Transcriptome sequencing service was provided by Biomarker Technologies (BMK), GmbH. Briefly, RNA were extracted from liver biopsies using Trizol reagent. The quality and quantity of extracted RNA was assessed by Nanodrop (quantity and purity) and Labchip GX (Quality). The cDNA libraries were prepared using Hieff NGS Ultima Dual-mode mRNA Library Prep Kit from Illumina (Yeasen) as per manufacturer's instructions. RNA sequencing was performed on NoveSeq6000 platform (PE 150 mode). For raw data processing, FastQC (v0.11.9) was used as a quality control check for raw sequencing. Alignment to the reference genome (GRCh38, Ensembl release 77) was performed using STAR (v2.7.9a), and gene expression levels (transcripts-per-million, TPM) were estimated using RSEM (v1.3.1). Gene expression data underwent a logarithmic transformation to log2(TPM + 1) and mean-centering normalization for downstream analyses.

Statistical analysis

All analyses in this study were conducted using R version 4.3.1. Linear regression model was used to evaluate the linear association between histological grades and molecular abundance levels with adjustment for age, sex, BMI, and diabetes. Statistically significantly changed metabolites or genes were defined by controlling the overall type I error at 5% or 10% (q value < 0.05 or 0.1). Spearman rank correlation was used to assess the relationship between the same metabolite in the liver and plasma. This accounts for matrix effects across different tissue types in untargeted analysis by comparing the relative intensity ranking of a metabolite across all samples within each tissue type. Gene overrepresentation analyses were performed using gene ontology recourse by in-house software [113]. ClueGO, a plugin app in Cytoscape, was used to visualize enrichment maps [114]. Partial correlation network analysis was employed to integrate the two omics layers using an in-house partial correlation network algorithm ACCORD [31]. KEGG pathway database was used for the analysis of lipid metabolism and pathway mapping [115]. All network visualizations in this study were done using Cytoscape [116].

To investigate MASLD subgroup signatures related to diabetic status, we analyzed linear associations between gene signatures and histological features separately in non-diabetic (n = 71) and diabetic individuals (n = 23). Statistical power was estimated by comparing variance explained in full (y ~ x + a + b + c) versus reduced (y ~ a + b + c) regression models, converting the incremental R^2 into Cohen's f^2, and applying pwr.f2.test at α = 0.05. We further compared gene expression profiles between diabetic (n = 21) and non-diabetic (n = 43) MASLD patients, identifying 166 differentially expressed genes ($p < 0.05$, $|\log_2 FC| > 0.32$). Of these, 54 genes (**Table S10**) were both differentially expressed and significantly associated with fibrosis progression, and thus marked as signatures in diabetic MASLD.

To identify progressive markers of liver fibrosis, we performed pairwise analyses for fibrosis stages using two distinct baselines: patients with no MASLD and those with steatosis but no fibrosis. 213 markers were characterized as progressive based on the following criteria: a) significant linear association with fibrosis grades, and b) significant differential expression (p value < 0.05 in t-test) in at least two fibrosis stages (e.g., F1 and F2, F2 and F3) compared to both baselines.

To identify independent gene signatures associated specifically with steatosis and fibrosis progression, we applied linear regression models for each outcome adjusting for the other. Steatosis-specific signatures were defined as genes significantly associated with steatosis but not with fibrosis, and vice versa. Metascape was used for meta-analysis of enrichment pathways [117]. Pathways with at least 10 hits and p value < 0.05 were considered steatosis- or fibrosis-specific.

For meta-analysis of reference human cohorts, the two RNA-seq datasets of the liver transcriptome, the VA cohort (GSE130970) and the EU cohort (GSE135251), were downloaded from Gene Expression Omnibus, and associations between gene expression (log2 TPM) and fibrosis grades or NAS were analyzed using linear regression. In the EU cohort, the patients without MASH diagnosis were removed from the meta-analysis for the purpose of identifying fibrosis signatures in MASH patients. Human liver single cell dataset was obtained from GSE115469 [63]. The mean log2 TPM was calculated for each cell type, and cell specificity was determined by subtracting the mean expression levels across all cell types.

Cross-referencing datasets of mouse models and human liver organoids

The RNA sequencing data (raw counts) for HSCs isolated from liver fibrosis mouse models [77] was downloaded from GSE176042 and analyzed using the DESeq2 R package. This previously published study investigated HSC initiation and perpetuation using acute and chronic models, respectively. For the acute model, mice were injected with CCl_4 once and samples were taken at 24 h, 72 h, and 1 w. For the chronic model, mice received a regimen of semi-weekly injection of CCl_4 for 4 weeks. After this regimen, mice were sacrificed and samples were taken at 24 h, 72 h, and 2 w. The statistical results from single cell dataset of stem cell-derived human liver organoids were obtained from GSE207889 [78].

3D liver spheroid MASH model

3D liver spheroids were generated based on co-cultures of cryopreserved primary human hepatocytes (PHH) and liver non-parenchymal cells (NPC) as previously described [75]. Briefly, cells were seeded at a PHH:NPC ratio of 6:1 in 96-well ultra-low attachment plates (CLS7007-24EA Corning) with a total of 1500 cells/well in culture medium (William's E medium containing 11 mM glucose, 100 nM dexamethasone,

10 μg/mL insulin, 5.5 mg/L transferrin, 6.7 μg/L selenite, 2 mM L-glutamine, 100 U/mL penicillin, 0.1 mg/mL streptomycin) supplemented with 10% FBS. After spheroid formation FBS was phased out and cells were maintained in medium supplemented with albumin-conjugated free-fatty acids (FFA) including 80μM palmitic acid and 80 μM oleic acid. At the end of the experiment, spheroids were collected for RNA extraction (Zymo R105). The elafibranor treatment protocol was described in the previous study [75]. Each experimental condition (control, MASH, and elafibranor treatment) was performed in quadruplicate.

Table 1. Patient characteristics

	Patients (N)	No MASLD (N = 33)	MASLD (N = 76)	P value
Patient information				
Age (years), median ± MAD	109	36 (14.8)	41.5 (9.6)	0.942
Sex (male), n (%)	108	4 (12.1)	22 (29.3)	0.092
Diabetes, n (%)	109	2 (6.1)	27 (35.5)	0.003
Hypertension, n (%)	93	6 (18.2)	16 (26.7)	0.505
BMI (kg/m2), median ± MAD	108	42.6 (6.6)	44.5 (9.1)	0.045
Clinical chemistry parameters				
ALT (U/L), median ± MAD	104	24 (11.9)	42 (25.2)	0.507
AST (U/L), median ± MAD	104	24 (7.4)	30 (13.3)	0.39
ALT/AST, median ± MAD	104	1 (0.3)	1.33 (0.4)	0.005
GGT (U/L), median ± MAD	104	23 (10.4)	28 (13.3)	0.041
Total cholesterol (mmol/L), median ± MAD	104	4 (0.9)	4.15 (1.0)	0.072
HDL (mmol/L), median ± MAD	102	1.04 (0.2)	0.94 (0.2)	0.053
LDL (mmol/L), median ± MAD	101	2.2 (0.7)	2.6 (0.7)	0.081
Non-HDL cholesterol (mmol/L), median ± MAD	108	2.76 (0.9)	3.27 (1.0)	0.003
Blood triglyceride (mmol/L), median ± MAD	103	1.2 (0.6)	1.5 (0.6)	0.013
Insulin (mU/L), median ± MAD	100	7.95 (5.6)	10.35 (7.1)	0.043
FBG (mmol/L), median ± MAD	102	4.9 (0.7)	5.2 (1.0)	0.114
C-peptide (nmol/L), median ± MAD	101	0.8 (0.4)	1.12 (0.4)	0.002
HOMA2–IR, median ± MAD	92	1.13 (0.7)	1.43 (0.9)	0.034
Liver histology				
Steatosis (S0/S1/S2/S3)	109	33/0/0/0	0/41/27/8	<0.001
Inflammation (I0/I1/I2/I3)	109	30/3/0/0	21/46/7/2	<0.001
Ballooning (B0/B1/B2)	109	33/0/0	65/10/1	0.07
NAS (N0/N1/N2/N3/ N4/N5/N6/N7)	109	30/3/0/0/ 0/0/0/0	0/15/29/13/ 14/2/2/1	<0.001
Fibrosis (F0/F1/F2/F3)	109	27/6/0/0	23/27/20/6	<0.001

MASLD: Metabolic dysfunction-associated steatotic liver disease; Median absolute deviation; BMI: Body mass index; ALT: Alanine transaminase; AST: Aspartate aminotransferase; GGT: Gamma-glutamyl transpeptidase; HOMA2 – IR: Homeostasis model assessment 2 of insulin resistance; HDL: High-density lipoprotein; LDL: Low-density lipoprotein; NAS: Nonalcoholic fatty liver disease activity score.

Figure legends

Figure 1: Study overview. (A) The overall study design. (B) Alluvial diagram of patient composition of groupings across liver histological features. (C) Relationship between clinical test results and stages of liver histological features. Node size was determined by –log10(p value) in ANOVA tests. Color indicates the significance degree [–log10(p value)] and the direction of change from early to late stages. (D) Number of metabolites analyzed in the liver and plasma. (E-F) Principal component analysis of liver metabolome, plasma metabolome, and liver transcriptome. (G) Disease spectra covered in this cohort and comparison to two published datasets.

Figure 2: Hepatic and circulating metabolome in obese individuals with MASLD. (A) Number of metabolites in each class that were significantly associated with histological features in the liver (q value < 0.05). Metabolite classes with at least 5 metabolites with significance are shown in the plot. (B) Associations between steatosis grades and lipid species in each lipid class. Dots were colored by double bond numbers (left) and carbon numbers (right) of lipid species, respectively. (C) Partial correlation network of the plasma metabolome and clinical covariates. Node size reflects the degree of connectivity, with larger nodes indicating connections to a greater number of metabolite nodes. (D) Heatmaps for pairwise analysis between plasma lipid classes and clinical variables. Linear regression analysis was performed for numerical variables, while logistic regression was conducted for binary variables. Significance values refer to –log10(p value)*sign(coefficients) from regression models. (E) Comparisons of liver metabolome and plasma metabolome regarding their associations with liver steatosis and fibrosis.

Figure 3: Integrative view of key metabolic pathways implicated in liver metabolism in obese individuals with MASLD. (A) Heatmap of log2 fold changes from pair-wise analysis of lipid metabolism-related genes. Association with steatosis (S) and fibrosis (F) is indicated by black dots (q value < 0.05, top). Results were cross-referenced with two published cohorts (VA cohort, GSE130970; EU cohort, GSE135251, bottom). Asterisks indicate genes with a q-value < 0.05 and a consistent change in direction within our cohort. (B) KEGG metabolic pathways with at least 4 genes or metabolites significantly associated with steatosis [S] or fibrosis [F]. (C) Integrative map of gene and metabolite alterations associated with steatosis (left half of each box/circle) and fibrosis (right half of each box/circle). (D) Metabolite alterations corresponding to the advancement of steatosis grades (x-axis).

Figure 4: Dysregulated mitochondrial function and autophagy during the progression of steatosis and fibrosis. Gene expression patterns related to mitochondrial metabolism (A), mitochondria-related biological processes (A), autophagy activation (B), and lysosomal biogenesis (B) with statistical association to steatosis and fibrosis. S, steatosis. F, fibrosis.

Figure 5: Steatosis and fibrosis as independent processes. (A) Network of genes, metabolites, and histological features (fibrosis and steatosis) using partial correlation analysis as described in the methods. (B) Venn diagrams depicting the number of genes significantly associated with steatosis and fibrosis (q value < 0.05). (C) Gene ontology (GO) enrichment of gene sets specific to steatosis or fibrosis.

Figure 6: Liver fibrosis signatures and potential therapeutic targets of fibrosis initiation. (A) Top 60 fibrosis markers in the liver. A total of 213 genes were identified, from which the top 30 upregulated and top 30 downregulated genes are visualized. The middle plot (blue bar on top) shows the comparison of individuals with fibrosis and without pathology (baseline - "no MASLD"). For the right plot (red bar), individuals with fibrosis were compared to those with steatosis but no fibrosis (baseline – "steatosis but no fibrosis"). Results were cross-referenced with two published cohorts (VA cohort, GSE130970; EU cohort, GSE135251, right). Asterisks indicate genes with a q-value < 0.05 and a consistent change in direction within our cohort. The average gene expressions of liver cell types were obtained from GSE115469 at the log2CPM level (left). Dots in the single cell map indicate zero expression in the corresponding cell types. (B) Enrichment of pathways in the transition from simple steatosis to the onset of fibrosis. (C) Protein-protein interaction network of GTPases and their regulators. Nodes are colored based on gene type, with borders indicating the direction of gene regulation. Node size corresponds to the significance of the genes in relation to fibrosis grades within this cohort. GEFs: Guanine nucleotide exchange factors. GAPs: GTPase-activating proteins. (D) Comparison of expression level changes in GTPase-related genes between this human cohort and an independent 3D spheroid MASH system. Log2 fold change for the human cohort was calculated by comparing patients with grade 2 or 3 fibrosis to those without fibrosis or steatosis. Genes with the same direction of change are colored in red, while others are colored in purple. (E) Expression of GTPase-related genes in patient-derived 3D liver spheroids: control spheroids, spheroids from patients with MASH, and Elafibranor-treated MASH spheroids (n = 4). Sixty-eight genes with a p-value < 0.05 from the ANOVA test were plotted in the diagram, with blue lines highlighting 24 genes that exhibited increased expression in the MASH group compared to the control group.

Acknowledgments

We thank all present and past members of the Watt, Choi, Lauschke, and Kaldis laboratories for discussions, input, and support. P.K. thanks Åke Nilsson for discussions and suggestions.

Abbreviations

ALT Alanine aminotransferase
AST Aspartate aminotransferase
ALP Alkaline phosphatase
CAR Acylcarnitines
CCl_4 Carbon tetrachloride
Cer Ceramide
CM Conditioned medium
CYP Cytochrome P
DAG/DG Diacylglycerol
DDA Data-dependent acquisition
ECM Extracellular matrix
FBS Fetal bovine serum
FFA Free-fatty acids
FXR Farnesoid X receptor
GAP GTPase-activating protein
GEF Guanine nucleotide exchange factor

GGT Gamma-glutamyltransferase
GL Glycerolipid
GPL Glycerophospholipid
HSC Hepatic stellate cell
HILIC Hydrophilic interaction liquid chromatography
LD Lipid droplet
LNAPE N-acyl-lysophosphatidylethanolamine
LPC-O Ether-linked lysophosphatidylcholine
LPI Ether-linked lysophosphatidylinositol
LPS Ether-linked lysophosphatidylserine
LPC Lysophosphatidylcholine
LPE Lysophosphatidylethanolamine
MG Monoacylglycerol
MASH Metabolic dysfunction-associated steatohepatitis
MASLD Metabolic dysfunction-associated steatotic liver disease
NAS NAFLD activity score
NPC Non-parenchymal cells
NAE N-acyl ethanolamines
PCA Principal component analysis
PHH Primary human hepatocytes
PUFA Polyunsaturated fatty acid
PC Phosphatidylcholine
PC-O Ether-linked phosphatidylcholine
PE Phosphatidylethanolamine
PE-O Ether-linked phosphatidylethanolamine
PG Phosphatidylglycerol
PI Phosphatidylinositol
PS Phosphatidylserine
QC Quality control
RP Reverse phase
SM Sphingomyelin
SL Sphingolipid
SPB Sphingoid base
TAG/TG Triacylglyceride
TAG-O Ether-linked triacylglycerol
Vitamin E Alpha-tocopherol

Conflict of interest statement:
VML is co-founder, CEO and shareholder of HepaPredict AB, as well as co-founder and shareholder of Shanghai Hepo Biotechnology Ltd. All other authors declare no conflict of interest.

Data availability
All data are available within the manuscript, supplemental figures, and supplemental tables. RNA sequencing data to this article have been submitted to SRA (PRJNA1185558) and is deposited with GEO (GSE281797). Untargeted LC-HRMS data is deposited with Zenodo, including IDA data (DOI 10.5281/zenodo.14091962), SWATH data for the organic fraction (DOI 10.5281/zenodo.14096635), and SWATH data for the aqueous fraction (DOI 10.5281/zenodo.14096753, DOI 10.5281/zenodo.14136832). All clinical data, processed omics datasets, and code are available at https://github.com/SLINGhub/MASLD_dual_omics.

Financial support statement:

PK is supported in part by the Novo Nordisk Foundation (NNF24OC0092365), Swedish Research Council (2021-01331), the Swedish Cancer Society (Cancerfonden; 21-1566Pj and 24-3605Pj), the Crafoord Foundation (Ref. No. 20220628), the Swedish Foundation for Strategic Research Dnr IRC15-0067, and Swedish Research Council, Strategic Research Area EXODIAB, Dnr 2009-1039. LNZ is supported in part by the IngaBritt och Arne Lundbergs Forskningsstiftelse LU2020-0013, the Crafoord Foundation (Ref. No. 20210516, Ref. No. 20220582), Stiftelsen Längmanska kulturfonden (BA21-0148), and the Åke Wibergs Stiftelse. VML acknowledges support from the Swedish Research Council (2021-02801 and 2023-03015), the Ruth och Richard Julins Foundation for Gastroenterology (2021-00158), Knut and Alice Wallenberg Foundation (VC-2021-0026), by the SciLifeLab and Wallenberg National Program for Data-Driven Life Science (WASPDDLS22:006), a Novo Nordisk Pioneer Innovator Grant (NNF23OC0085944), the Robert Bosch Foundation, as well as the Innovative Medicines Initiative 2 Joint Undertaking (JU) under grant agreement No. 875510. The JU receives support from the European Union's Horizon 2020 research and innovation programme and EFPIA, Ontario Institute for Cancer Research, Royal Institution for the Advancement of Learning McGill University, Kungliga Tekniska Hoegskolan, and Diamond Light Source Limited. HC is supported in part by Singapore Ministry of Education (T2EP202121-0016, T2EP20223-0010), National Research Foundation and Agency for Science, Technology and Research (I1901E0040), and National Medical Research Council (CG21APR1008). MJW is supported by the National Health and Medical Research Council of Australia (APP1162511). The funders had no role in study design, data collection and interpretation, or the decision to submit the work for publication.

Author contributions:

QZ*: designing research studies, conducting experiments, acquiring data, analyzing data, writing the manuscript
WD*: designing research studies, conducting experiments, acquiring data, analyzing data, writing the manuscript
RW*: analyzing data, writing the manuscript
YZ: conducting experiments, acquiring data, analyzing data
UK: analyzing data, writing the manuscript
LNZ: analyzing data, writing the manuscript
HT: conducting experiments, acquiring data, analyzing data
SY: conducting experiments, acquiring data, analyzing data
MY: conducting experiments, acquiring data, analyzing data
YX: conducting experiments, acquiring data, analyzing data
YK: conducting experiments, acquiring data, analyzing data
SL: conducting experiments, acquiring data, analyzing data
RL: conducting experiments, acquiring data, analyzing data
GT: conducting experiments, acquiring data, analyzing data
PN: conducting experiments, acquiring data, analyzing data
PRB: providing reagents, cohort management
VMK: designing research studies, analyzing data, writing the manuscript, supervision, funding acquisition
HC: designing research studies, analyzing data, writing the manuscript, supervision, funding acquisition

MJW: designing research studies, analyzing data, writing the manuscript, supervision, funding acquisition
PK: designing research studies, analyzing data, writing the manuscript, supervision, funding acquisition, leading of collaboration

QZ, WD, and RW are co-first authors based on their contributions, which was writing original draft, LC-MS data acquisition and bioinformatic analysis of transcriptomic, metabolomic, and clinical data (QZ), organizing cohort samples, clinical parameters, managing, and LX-2 experiments (WD), and writing the original draft and analyzing data (RW).

References

1. Miao L, Targher G, Byrne CD, et al. Current status and future trends of the global burden of MASLD. Trends Endocrinol Metab 2024;35:697-707.
2. Riazi K, Azhari H, Charette JH, et al. The prevalence and incidence of NAFLD worldwide: a systematic review and meta-analysis. Lancet Gastroenterol Hepatol 2022;7:851-861.
3. Targher G, Byrne CD, Tilg H. MASLD: a systemic metabolic disorder with cardiovascular and malignant complications. Gut 2024;73:691-702.
4. Yki-Jarvinen H. Non-alcoholic fatty liver disease as a cause and a consequence of metabolic syndrome. Lancet Diabetes Endocrinol 2014;2:901-10.
5. Angulo P, Kleiner DE, Dam-Larsen S, et al. Liver Fibrosis, but No Other Histologic Features, Is Associated With Long-term Outcomes of Patients With Nonalcoholic Fatty Liver Disease. Gastroenterology 2015;149:389-97.e10.
6. Ekstedt M, Hagström H, Nasr P, et al. Fibrosis stage is the strongest predictor for disease-specific mortality in NAFLD after up to 33 years of follow-up. Hepatology 2015;61:1547-54.
7. Hagstrom H, Nasr P, Ekstedt M, et al. Fibrosis stage but not NASH predicts mortality and time to development of severe liver disease in biopsy-proven NAFLD. J Hepatol 2017;67:1265-1273.
8. Rodriguez LA, Schmittdiel JA, Liu L, et al. Hepatocellular Carcinoma in Metabolic Dysfunction-Associated Steatotic Liver Disease. JAMA Netw Open 2024;7:e2421019.
9. Feng G, Valenti L, Wong VW, et al. Recompensation in cirrhosis: unravelling the evolving natural history of nonalcoholic fatty liver disease. Nat Rev Gastroenterol Hepatol 2024;21:46-56.
10. Eslam M, Newsome PN, Sarin SK, et al. A new definition for metabolic dysfunction-associated fatty liver disease: An international expert consensus statement. J Hepatol 2020;73:202-209.
11. Scoditti E, Sabatini S, Carli F, et al. Hepatic glucose metabolism in the steatotic liver. Nat Rev Gastroenterol Hepatol 2024;21:319-334.
12. Lambert JE, Ramos-Roman MA, Browning JD, et al. Increased de novo lipogenesis is a distinct characteristic of individuals with nonalcoholic fatty liver disease. Gastroenterology 2014;146:726-35.
13. Sakuma I, Gaspar RC, Nasiri AR, et al. Liver lipid droplet cholesterol content is a key determinant of metabolic dysfunction-associated steatohepatitis. Proc Natl Acad Sci U S A 2025;122:e2502978122.
14. Koliaki C, Szendroedi J, Kaul K, et al. Adaptation of hepatic mitochondrial function in humans with non-alcoholic fatty liver is lost in steatohepatitis. Cell Metab 2015;21:739-46.
15. Fromenty B, Roden M. Mitochondrial alterations in fatty liver diseases. J Hepatol 2023;78:415-429.
16. Bril F, Barb D, Portillo-Sanchez P, et al. Metabolic and histological implications of intrahepatic triglyceride content in nonalcoholic fatty liver disease. Hepatology 2017;65:1132-1144.
17. Younossi Z, Anstee QM, Marietti M, et al. Global burden of NAFLD and NASH: trends, predictions, risk factors and prevention. Nat Rev Gastroenterol Hepatol 2018;15:11-20.

18. Vvedenskaya O, Rose TD, Knittelfelder O, et al. Nonalcoholic fatty liver disease stratification by liver lipidomics. J Lipid Res 2021;62:100104.
19. McGlinchey AJ, Govaere O, Geng D, et al. Metabolic signatures across the full spectrum of non-alcoholic fatty liver disease. JHEP Rep 2022;4:100477.
20. Angulo P, Kleiner DE, Dam-Larsen S, et al. Liver Fibrosis, but No Other Histologic Features, Is Associated With Long-term Outcomes of Patients With Nonalcoholic Fatty Liver Disease. Gastroenterology 2015;149:389-97 e10.
21. Bataller R, Brenner DA. Liver fibrosis. J Clin Invest 2005;115:209-18.
22. Subramanian P, Hampe J, Tacke F, et al. Fibrogenic Pathways in Metabolic Dysfunction Associated Fatty Liver Disease (MAFLD). Int J Mol Sci 2022;23:6996.
23. Powell EE, Wong VW, Rinella M. Non-alcoholic fatty liver disease. Lancet 2021;397:2212-2224.
24. European Association for the Study of the Liver . Electronic address eee, European Association for the Study of D, European Association for the Study of O, et al. EASL-EASD-EASO Clinical Practice Guidelines on the management of metabolic dysfunction-associated steatotic liver disease (MASLD). J Hepatol 2024;81:492-542.
25. Rinella ME, Neuschwander-Tetri BA, Siddiqui MS, et al. AASLD Practice Guidance on the clinical assessment and management of nonalcoholic fatty liver disease. Hepatology 2023;77:1797-1835.
26. Hoang SA, Oseini A, Feaver RE, et al. Gene Expression Predicts Histological Severity and Reveals Distinct Molecular Profiles of Nonalcoholic Fatty Liver Disease. Sci Rep 2019;9:12541.
27. Govaere O, Cockell S, Tiniakos D, et al. Transcriptomic profiling across the nonalcoholic fatty liver disease spectrum reveals gene signatures for steatohepatitis and fibrosis. Sci Transl Med 2020;12:eaba4448.
28. Govaere O, Hasoon M, Alexander L, et al. A proteo-transcriptomic map of non-alcoholic fatty liver disease signatures. Nat Metab 2023;5:572-578.
29. Roumans KHM, Lindeboom L, Veeraiah P, et al. Hepatic saturated fatty acid fraction is associated with de novo lipogenesis and hepatic insulin resistance. Nat Commun 2020;11:1891.
30. Wang D, Wei Y, Pagliassotti MJ. Saturated fatty acids promote endoplasmic reticulum stress and liver injury in rats with hepatic steatosis. Endocrinology 2006;147:943-51.
31. Lee S, Bang J, Kim Y, et al. Learning Massive-scale Partial Correlation Networks in Clinical Multi-omics Studies with HP-ACCORD. arXiv preprint arXiv:2412.11554 2024.
32. Huang Q, Qadri SF, Bian H, et al. A metabolome-derived score predicts metabolic dysfunction-associated steatohepatitis and mortality from liver disease. J Hepatol 2025;82:781-793.
33. Lahdou I, Sadeghi M, Oweira H, et al. Increased serum levels of quinolinic acid indicate enhanced severity of hepatic dysfunction in patients with liver cirrhosis. Hum Immunol 2013;74:60-6.
34. Gou Y, Li A, Dong X, et al. Lactate transporter MCT4 regulates the hub genes for lipid metabolism and inflammation to attenuate intracellular lipid accumulation in non-alcoholic fatty liver disease. Genes Dis 2025;12:101554.
35. Tan Q, Deng S, Xiong L. Role of Kynurenine and Its Derivatives in Liver Diseases: Recent Advances and Future Clinical Perspectives. Int J Mol Sci 2025;26.

36. Mashek DG. Hepatic lipid droplets: A balancing act between energy storage and metabolic dysfunction in NAFLD. Mol Metab 2021;50:101115.
37. Holdaway CM, Leonard KA, Nelson R, et al. Alterations in phosphatidylethanolamine metabolism impacts hepatocellular lipid storage, energy homeostasis, and proliferation. Biochim Biophys Acta Mol Cell Biol Lipids 2025;1870:159608.
38. van der Veen JN, Lingrell S, Vance DE. The membrane lipid phosphatidylcholine is an unexpected source of triacylglycerol in the liver. J Biol Chem 2012;287:23418-26.
39. Dos Santos LRB, Fleming I. Role of cytochrome P450-derived, polyunsaturated fatty acid mediators in diabetes and the metabolic syndrome. Prostaglandins Other Lipid Mediat 2020;148:106407.
40. Hajeyah AA, Griffiths WJ, Wang Y, et al. The Biosynthesis of Enzymatically Oxidized Lipids. Front Endocrinol (Lausanne) 2020;11:591819.
41. Albaugh VL, Mukherjee K, Barbul A. Proline Precursors and Collagen Synthesis: Biochemical Challenges of Nutrient Supplementation and Wound Healing. J Nutr 2017;147:2011-2017.
42. de Paz-Lugo P, Lupianez JA, Melendez-Hevia E. High glycine concentration increases collagen synthesis by articular chondrocytes in vitro: acute glycine deficiency could be an important cause of osteoarthritis. Amino Acids 2018;50:1357-1365.
43. Schnabl B, Damman CJ, Carr RM. Metabolic dysfunction-associated steatotic liver disease and the gut microbiome: pathogenic insights and therapeutic innovations. J Clin Invest 2025;135.
44. Yanko R, Levashov M, Chaka OG, et al. Tryptophan Prevents the Development of Non-Alcoholic Fatty Liver Disease. Diabetes Metab Syndr Obes 2023;16:4195-4204.
45. Arto C, Rusu EC, Clavero-Mestres H, et al. Metabolic profiling of tryptophan pathways: Implications for obesity and metabolic dysfunction-associated steatotic liver disease. Eur J Clin Invest 2024;54:e14279.
46. Walker AK. 1-Carbon Cycle Metabolites Methylate Their Way to Fatty Liver. Trends Endocrinol Metab 2017;28:63-72.
47. Varela-Rey M, Martinez-Lopez N, Fernandez-Ramos D, et al. Fatty liver and fibrosis in glycine N-methyltransferase knockout mice is prevented by nicotinamide. Hepatology 2010;52:105-14.
48. Robinson AE, Binek A, Ramani K, et al. Hyperphosphorylation of hepatic proteome characterizes nonalcoholic fatty liver disease in S-adenosylmethionine deficiency. iScience 2023;26:105987.
49. Alarcon-Vila C, Insausti-Urkia N, Torres S, et al. Dietary and genetic disruption of hepatic methionine metabolism induce acid sphingomyelinase to promote steatohepatitis. Redox Biol 2023;59:102596.
50. Matthews RP, Lorent K, Manoral-Mobias R, et al. TNFalpha-dependent hepatic steatosis and liver degeneration caused by mutation of zebrafish S-adenosylhomocysteine hydrolase. Development 2009;136:865-75.
51. Sousa AP, Cunha DM, Franco C, et al. Which Role Plays 2-Hydroxybutyric Acid on Insulin Resistance? Metabolites 2021;11.
52. Knottnerus SJG, Bleeker JC, Wust RCI, et al. Disorders of mitochondrial long-chain fatty acid oxidation and the carnitine shuttle. Rev Endocr Metab Disord 2018;19:93-106.

53. Houten SM, Violante S, Ventura FV, et al. The Biochemistry and Physiology of Mitochondrial Fatty Acid beta-Oxidation and Its Genetic Disorders. Annu Rev Physiol 2016;78:23-44.
54. Rath S, Sharma R, Gupta R, et al. MitoCarta3.0: an updated mitochondrial proteome now with sub-organelle localization and pathway annotations. Nucleic Acids Res 2021;49:D1541-D1547.
55. Trivedi P, Wang S, Friedman SL. The Power of Plasticity-Metabolic Regulation of Hepatic Stellate Cells. Cell Metab 2021;33:242-257.
56. Martinez-Lopez N, Singh R. Autophagy and Lipid Droplets in the Liver. Annu Rev Nutr 2015;35:215-37.
57. Xie C, Woollett LA, Turley SD, et al. Fatty acids differentially regulate hepatic cholesteryl ester formation and incorporation into lipoproteins in the liver of the mouse. J Lipid Res 2002;43:1508-19.
58. Min HK, Kapoor A, Fuchs M, et al. Increased hepatic synthesis and dysregulation of cholesterol metabolism is associated with the severity of nonalcoholic fatty liver disease. Cell Metab 2012;15:665-74.
59. Kang Q, Chen A. Curcumin eliminates oxidized LDL roles in activating hepatic stellate cells by suppressing gene expression of lectin-like oxidized LDL receptor-1. Lab Invest 2009;89:1275-90.
60. Tuohetahuntila M, Molenaar MR, Spee B, et al. Lysosome-mediated degradation of a distinct pool of lipid droplets during hepatic stellate cell activation. J Biol Chem 2017;292:12436-12448.
61. Bordi M, De Cegli R, Testa B, et al. A gene toolbox for monitoring autophagy transcription. Cell Death Dis 2021;12:1044.
62. Singh R, Kaushik S, Wang Y, et al. Autophagy regulates lipid metabolism. Nature 2009;458:1131-5.
63. MacParland SA, Liu JC, Ma XZ, et al. Single cell RNA sequencing of human liver reveals distinct intrahepatic macrophage populations. Nat Commun 2018;9:4383.
64. Li Y, Fan W, Link F, et al. Transforming growth factor beta latency: A mechanism of cytokine storage and signalling regulation in liver homeostasis and disease. JHEP Rep 2022;4:100397.
65. Wen X, Liu Y, Bai Y, et al. LOXL2, a copper-dependent monoamine oxidase, activates lung fibroblasts through the TGF-beta/Smad pathway. Int J Mol Med 2018;42:3530-3541.
66. Munger JS, Huang X, Kawakatsu H, et al. The integrin alpha v beta 6 binds and activates latent TGF beta 1: a mechanism for regulating pulmonary inflammation and fibrosis. Cell 1999;96:319-28.
67. Kisseleva T, Brenner D. Molecular and cellular mechanisms of liver fibrosis and its regression. Nat Rev Gastroenterol Hepatol 2021;18:151-166.
68. Massague J, Sheppard D. TGF-beta signaling in health and disease. Cell 2023;186:4007-4037.
69. Go CD, Knight JDR, Rajasekharan A, et al. A proximity-dependent biotinylation map of a human cell. Nature 2021;595:120-124.
70. Razick S, Magklaras G, Donaldson IM. iRefIndex: a consolidated protein interaction database with provenance. BMC Bioinformatics 2008;9:405.
71. Huttlin EL, Bruckner RJ, Paulo JA, et al. Architecture of the human interactome defines protein communities and disease networks. Nature 2017;545:505-509.

72. Bell CC, Hendriks DF, Moro SM, et al. Characterization of primary human hepatocyte spheroids as a model system for drug-induced liver injury, liver function and disease. Sci Rep 2016;6:25187.
73. Vorrink SU, Ullah S, Schmidt S, et al. Endogenous and xenobiotic metabolic stability of primary human hepatocytes in long-term 3D spheroid cultures revealed by a combination of targeted and untargeted metabolomics. FASEB J 2017;31:2696-2708.
74. Kemas AM, Youhanna S, Zandi Shafagh R, et al. Insulin-dependent glucose consumption dynamics in 3D primary human liver cultures measured by a sensitive and specific glucose sensor with nanoliter input volume. FASEB J 2021;35:e21305.
75. Youhanna S, Kemas AM, Wright SC, et al. Chemogenomic Screening in a Patient-Derived 3D Fatty Liver Disease Model Reveals the CHRM1-TRPM8 Axis as a Novel Module for Targeted Intervention. Adv Sci (Weinh) 2025;12:e2407572.
76. Ratziu V, Harrison SA, Francque S, et al. Elafibranor, an Agonist of the Peroxisome Proliferator-Activated Receptor-alpha and -delta, Induces Resolution of Nonalcoholic Steatohepatitis Without Fibrosis Worsening. Gastroenterology 2016;150:1147-1159 e5.
77. De Smet V, Eysackers N, Merens V, et al. Initiation of hepatic stellate cell activation extends into chronic liver disease. Cell Death Dis 2021;12:1110.
78. Hess A, Gentile SD, Ben Saad A, et al. Single-cell transcriptomics stratifies organoid models of metabolic dysfunction-associated steatotic liver disease. EMBO J 2023;42:e113898.
79. Haag M, Winter S, Kemas AM, et al. Circulating metabolite signatures indicate differential gut-liver crosstalk in lean and obese MASLD. JCI Insight 2025;10.
80. Barr J, Caballeria J, Martinez-Arranz I, et al. Obesity-dependent metabolic signatures associated with nonalcoholic fatty liver disease progression. J Proteome Res 2012;11:2521-32.
81. Leszczynska A, Stoess C, Sung H, et al. Extracellular Vesicles as Therapeutic and Diagnostic Tools for Chronic Liver Diseases. Biomedicines 2023;11:2808.
82. Liu J, Hu S, Chen L, et al. Profiling the genome and proteome of metabolic dysfunction-associated steatotic liver disease identifies potential therapeutic targets. medRxiv. 2023:DOI: 10.1101/2023.11.30.23299247.
83. Radosavljevic T, Brankovic M, Samardzic J, et al. Altered Mitochondrial Function in MASLD: Key Features and Promising Therapeutic Approaches. Antioxidants 2024;13:906.
84. Saliba-Gustafsson P, Justesen JM, Ranta A, et al. A functional genomic framework to elucidate novel causal metabolic dysfunction-associated fatty liver disease genes. Hepatology 2024:: in press.
85. Scorletti E, Carr RM. A new perspective on NAFLD: Focusing on lipid droplets. J Hepatol 2022;76:934-945.
86. Van Woerkom A, Harney DJ, Nagarajan SR, et al. Hepatic lipid droplet-associated proteome changes distinguish dietary-induced fatty liver from glucose tolerance in male mice. Am J Physiol Endocrinol Metab 2024;326:E842-E855.
87. Carr RM, Patel RT, Rao V, et al. Reduction of TIP47 improves hepatic steatosis and glucose homeostasis in mice. Am J Physiol Regul Integr Comp Physiol 2012;302:R996-1003.

88. Babiy B, Ramos-Molina B, Ocana L, et al. Dihydrosphingolipids are associated with steatosis and increased fibrosis damage in non-alcoholic fatty liver disease. Biochim Biophys Acta Mol Cell Biol Lipids 2023;1868:159318.
89. Ooi GJ, Meikle PJ, Huynh K, et al. Hepatic lipidomic remodeling in severe obesity manifests with steatosis and does not evolve with non-alcoholic steatohepatitis. J Hepatol 2021;75:524-535.
90. Wei W, Lyu X, Markhard AL, et al. PTER is a N-acetyltaurine hydrolase that regulates feeding and obesity. Nature 2024;633:182-188.
91. Al-Baiaty FDR, Ismail A, Abdul Latiff Z, et al. Possible Hepatoprotective Effect of Tocotrienol-Rich Fraction Vitamin E in Non-alcoholic Fatty Liver Disease in Obese Children and Adolescents. Front Pediatr 2021;9:667247.
92. Arroyave-Ospina JC, Wu Z, Geng Y, et al. Role of Oxidative Stress in the Pathogenesis of Non-Alcoholic Fatty Liver Disease: Implications for Prevention and Therapy. Antioxidants 2021;10:174.
93. Aggarwal S, Yadav V, Maiwall R, et al. Metabolomic analysis shows dysregulation in amino acid and NAD+ metabolism in palmitate treated hepatocytes and plasma of non-alcoholic fatty liver disease spectrum. Biochem Biophys Res Commun 2023;643:129-138.
94. Xue C, Li G, Zheng Q, et al. Tryptophan metabolism in health and disease. Cell Metab 2023;35:1304-1326.
95. Gual P, Gilgenkrantz H, Lotersztajn S. Autophagy in chronic liver diseases: the two faces of Janus. Am J Physiol Cell Physiol 2017;312:C263-C273.
96. Adeva-Andany MM, Carneiro-Freire N, Seco-Filgueira M, et al. Mitochondrial beta-oxidation of saturated fatty acids in humans. Mitochondrion 2019;46:73-90.
97. Gray JL, von Delft F, Brennan PE. Targeting the Small GTPase Superfamily through Their Regulatory Proteins. Angew Chem Int Ed Engl 2020;59:6342-6366.
98. Bos JL, Rehmann H, Wittinghofer A. GEFs and GAPs: critical elements in the control of small G proteins. Cell 2007;129:865-77.
99. Huang H, Lee SH, Sousa-Lima I, et al. Rho-kinase/AMPK axis regulates hepatic lipogenesis during overnutrition. J Clin Invest 2018;128:5335-5350.
100. Schwerbel K, Kamitz A, Krahmer N, et al. Immunity-related GTPase induces lipophagy to prevent excess hepatic lipid accumulation. J Hepatol 2020;73:771-782.
101. Peng Y, Zeng Q, Wan L, et al. GP73 is a TBC-domain Rab GTPase-activating protein contributing to the pathogenesis of non-alcoholic fatty liver disease without obesity. Nat Commun 2021;12:7004.
102. Agarwal H, Wang Y, Ozcan L. Rap1 Activation Protects Against Fatty Liver and Non-Alcoholic Steatohepatitis Development. bioRxiv. 2023:DOI 10.1101/2023.10.24.563728.
103. Castane H, Jimenez-Franco A, Hernandez-Aguilera A, et al. Multi-omics profiling reveals altered mitochondrial metabolism in adipose tissue from patients with metabolic dysfunction-associated steatohepatitis. EBioMedicine 2025;111:105532.
104. Raverdy V, Tavaglione F, Chatelain E, et al. Data-driven cluster analysis identifies distinct types of metabolic dysfunction-associated steatotic liver disease. Nat Med 2024;30:3624-3633.

105. Chalasani N, Younossi Z, Lavine JE, et al. The diagnosis and management of nonalcoholic fatty liver disease: Practice guidance from the American Association for the Study of Liver Diseases. Hepatology 2017;67:328-357.
106. Saunders JB, Aasland OG, Babor TF, et al. Development of the Alcohol Use Disorders Identification Test (AUDIT): WHO Collaborative Project on Early Detection of Persons with Harmful Alcohol Consumption--II. Addiction 1993;88:791-804.
107. Brunt EM, Kleiner DE, Wilson LA, et al. Nonalcoholic fatty liver disease (NAFLD) activity score and the histopathologic diagnosis in NAFLD: distinct clinicopathologic meanings. Hepatology 2011;53:810-20.
108. Kleiner DE, Brunt EM, Van Natta M, et al. Design and validation of a histological scoring system for nonalcoholic fatty liver disease. Hepatology 2005;41:1313-21.
109. Wu ZE, Kruger MC, Cooper GJS, et al. Tissue-Specific Sample Dilution: An Important Parameter to Optimise Prior to Untargeted LC-MS Metabolomics. Metabolites 2019;9:124.
110. Xu J, Begley P, Church SJ, et al. Graded perturbations of metabolism in multiple regions of human brain in Alzheimer's disease: Snapshot of a pervasive metabolic disorder. Biochim Biophys Acta 2016;1862:1084-92.
111. Lee DY, Kind T, Yoon YR, et al. Comparative evaluation of extraction methods for simultaneous mass-spectrometric analysis of complex lipids and primary metabolites from human blood plasma. Anal Bioanal Chem 2014;406:7275-86.
112. Narayanaswamy P, Teo G, Ow JR, et al. MetaboKit: a comprehensive data extraction tool for untargeted metabolomics. Mol Omics 2020;16:436-447.
113. Gene Ontology C, Aleksander SA, Balhoff J, et al. The Gene Ontology knowledgebase in 2023. Genetics 2023;224:iyad031.
114. Bindea G, Mlecnik B, Hackl H, et al. ClueGO: a Cytoscape plug-in to decipher functionally grouped gene ontology and pathway annotation networks. Bioinformatics 2009;25:1091-3.
115. Kanehisa M, Sato Y, Kawashima M, et al. KEGG as a reference resource for gene and protein annotation. Nucleic Acids Res 2016;44:D457-62.
116. Otasek D, Morris JH, Boucas J, et al. Cytoscape Automation: empowering workflow-based network analysis. Genome Biol 2019;20:185.
117. Zhou Y, Zhou B, Pache L, et al. Metascape provides a biologist-oriented resource for the analysis of systems-level datasets. Nat Commun 2019;10:1523.

Graphical abstract

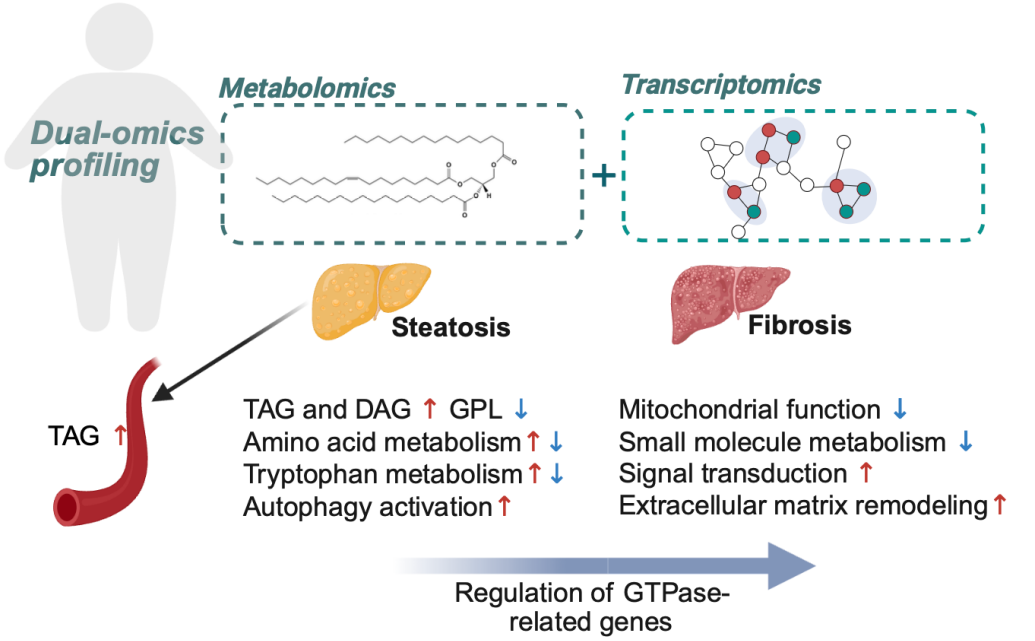

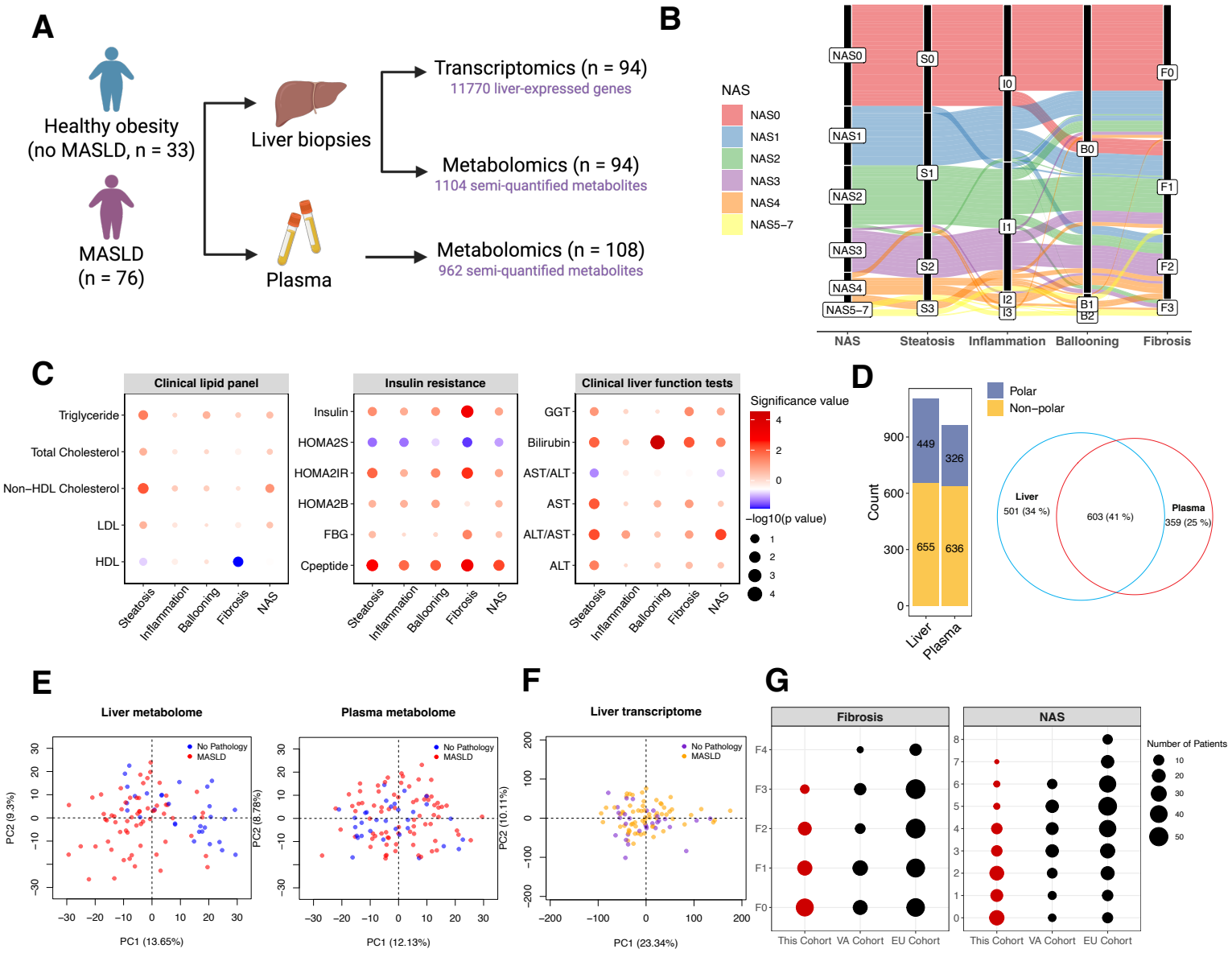

Figure 1. Study overview

(A) The overall study design. (B) Alluvial diagram of patient composition of groupings across liver histological features. (C) Relationship between clinical test results and stages of liver histological features. Node size was determined by –log10(p value) in ANOVA tests. Color indicates the significance degree [–log10(p value)] and the direction of change from early to late stages. (D) Number of metabolites analyzed in the liver and plasma. (E-F) Principal component analysis of liver metabolome, plasma metabolome, and liver transcriptome. (G) Disease spectra covered in this cohort and comparision to two published datasets.

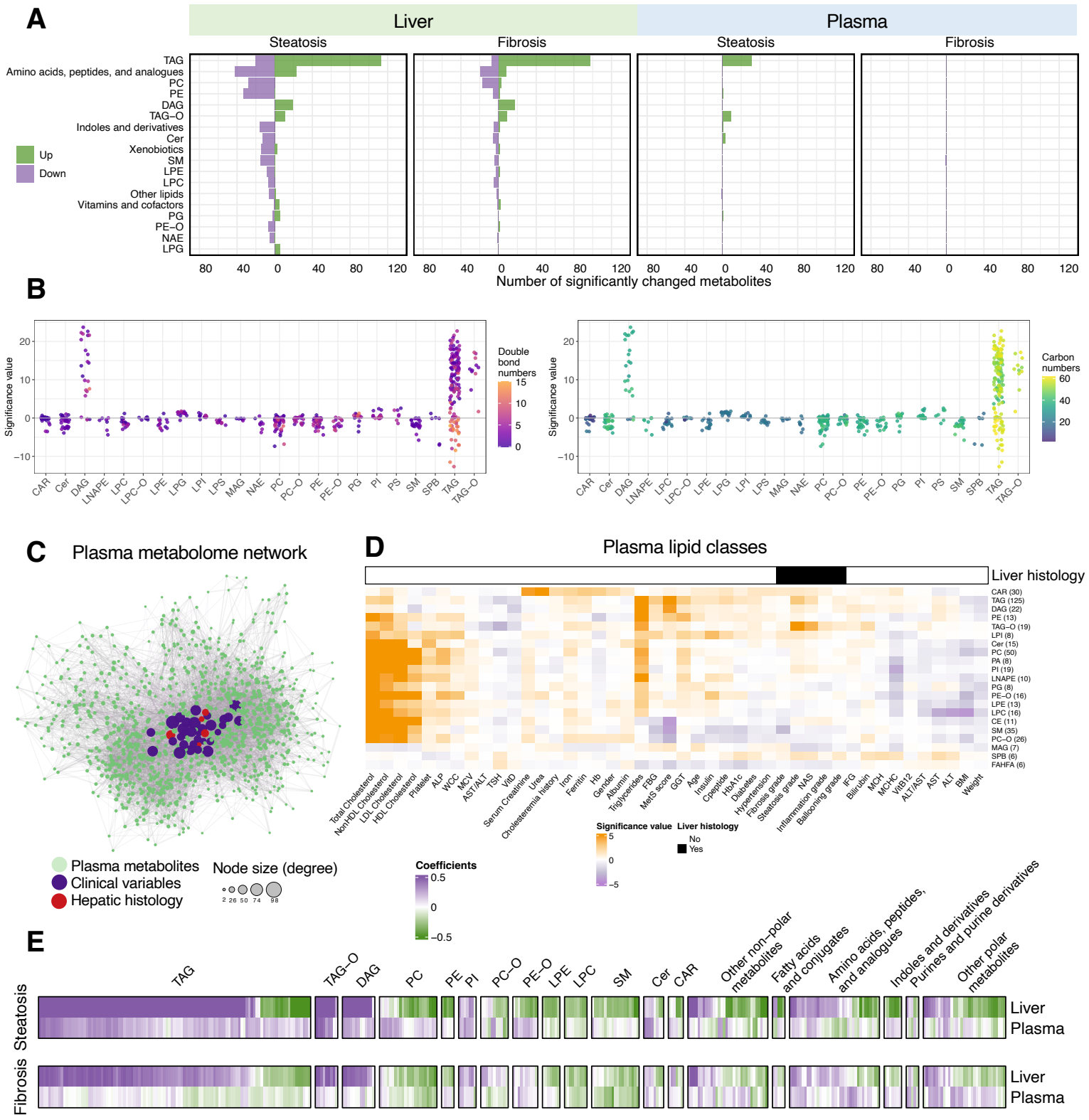

Figure 2. Hepatic and circulating metabolome in obese MASLD patients
(A) Number of metabolites in each class that were significantly associated with histological features in the liver (q value < 0.05). Metabolite classes with at least 5 metabolites with significance are shown in the plot. (B) Associations between steatosis grades and lipid species in each lipid class. Dots were colored by double bond numbers (left) and carbon numbers (right) of lipid species, respectively. (C) Partial correlation network of the plasma metabolome and clinical covariates. Node size reflects the degree of connectivity, with larger nodes indicating connections to a greater number of metabolite nodes. (D) Heatmaps for pairwise analysis between plasma lipid classes and clinical variables. Linear regression analysis was performed for numerical variables, while logistic regression was conducted for binary variables. Significance values refer to –log10(p value)*sign(coefficients) from regression models. (E) Comparisons of liver metabolome and plasma metabolome regarding their associations with liver steatosis and fibrosis.

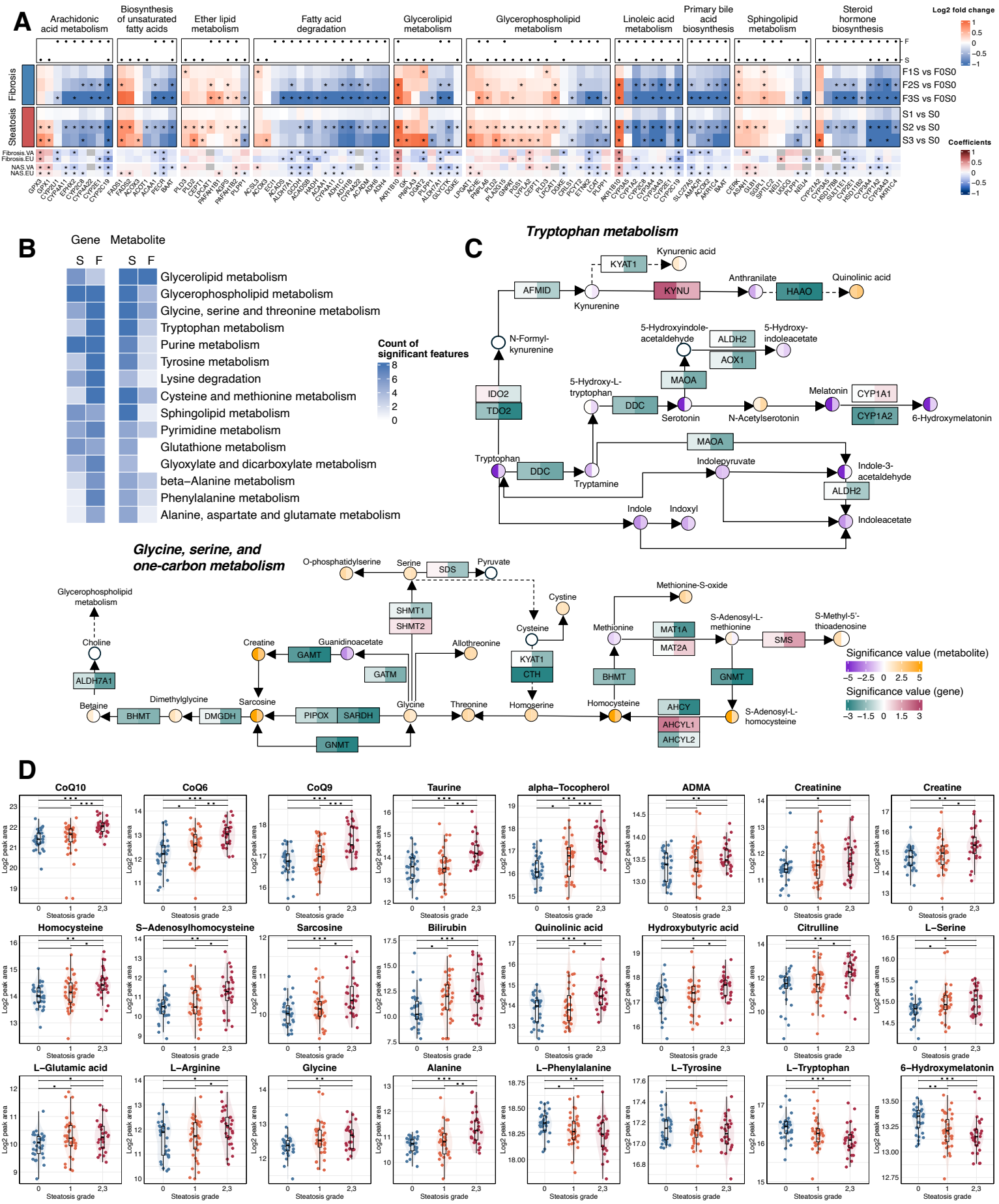

Figure 3. Integrative view of key metabolic pathways implicated in liver metabolism in obese individuals with MASLD
(A) Heatmap of log2 fold changes from pair-wise analysis of lipid metabolism-related genes. Association with steatosis (S) and fibrosis (F) is indicated by black dots (q value < 0.05, top). Results were cross-referenced with two published cohorts (VA cohort, GSE130970; EU cohort, GSE135251, bottom) Asterisks indicate genes with a q-value < 0.05 and a consistent change in direction within our cohort. (B) KEGG metabolic pathways with at least 4 genes or metabolites significantly associated with steatosis (S) or fibrosis (F). (C) Integrative map of gene and metabolite alterations associated with steatosis (left half of each box/circle) and fibrosis (right half of each box/circle). (D) Metabolite alterations corresponding to the advancement of steatosis grades (x-axis).

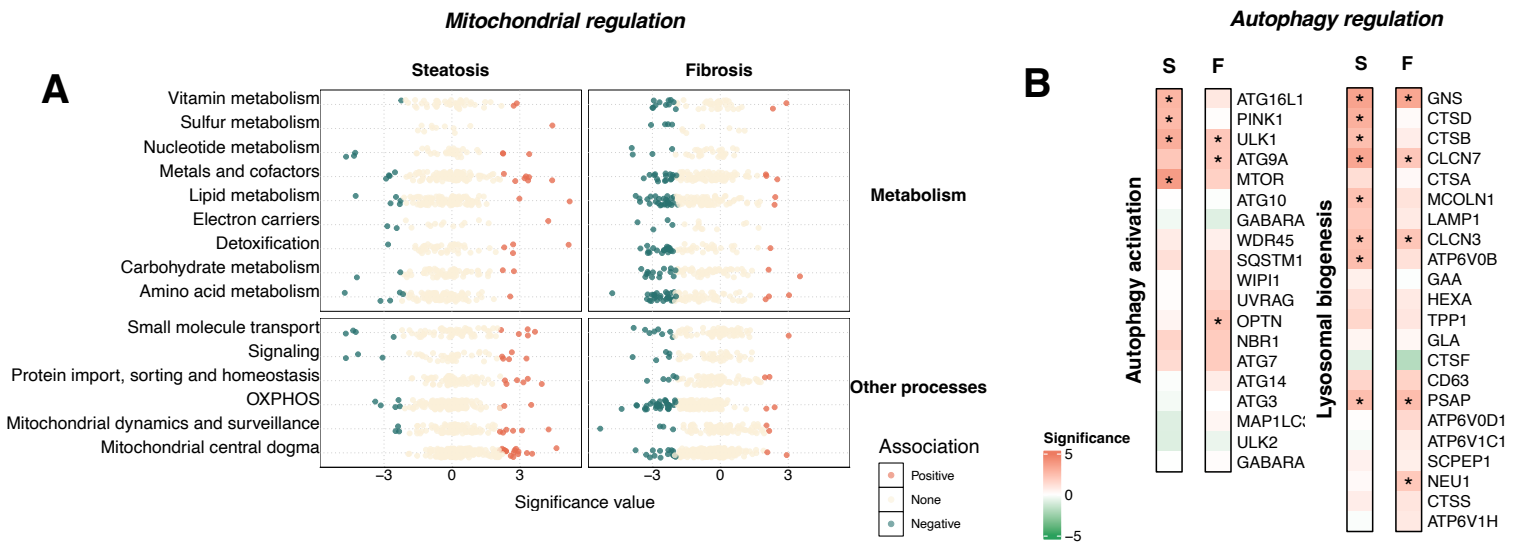

Figure 4. **Dysregulated mitochondrial function and autophagy during the progression of steatosis and fibrosis.** Gene expression patterns related to mitochondrial metabolism (A), mitochondria-related biological processes (A), autophagy activation (B), and lysosomal biogenesis (B) with statistical association to steatosis and fibrosis. S, steatosis. F, fibrosis.

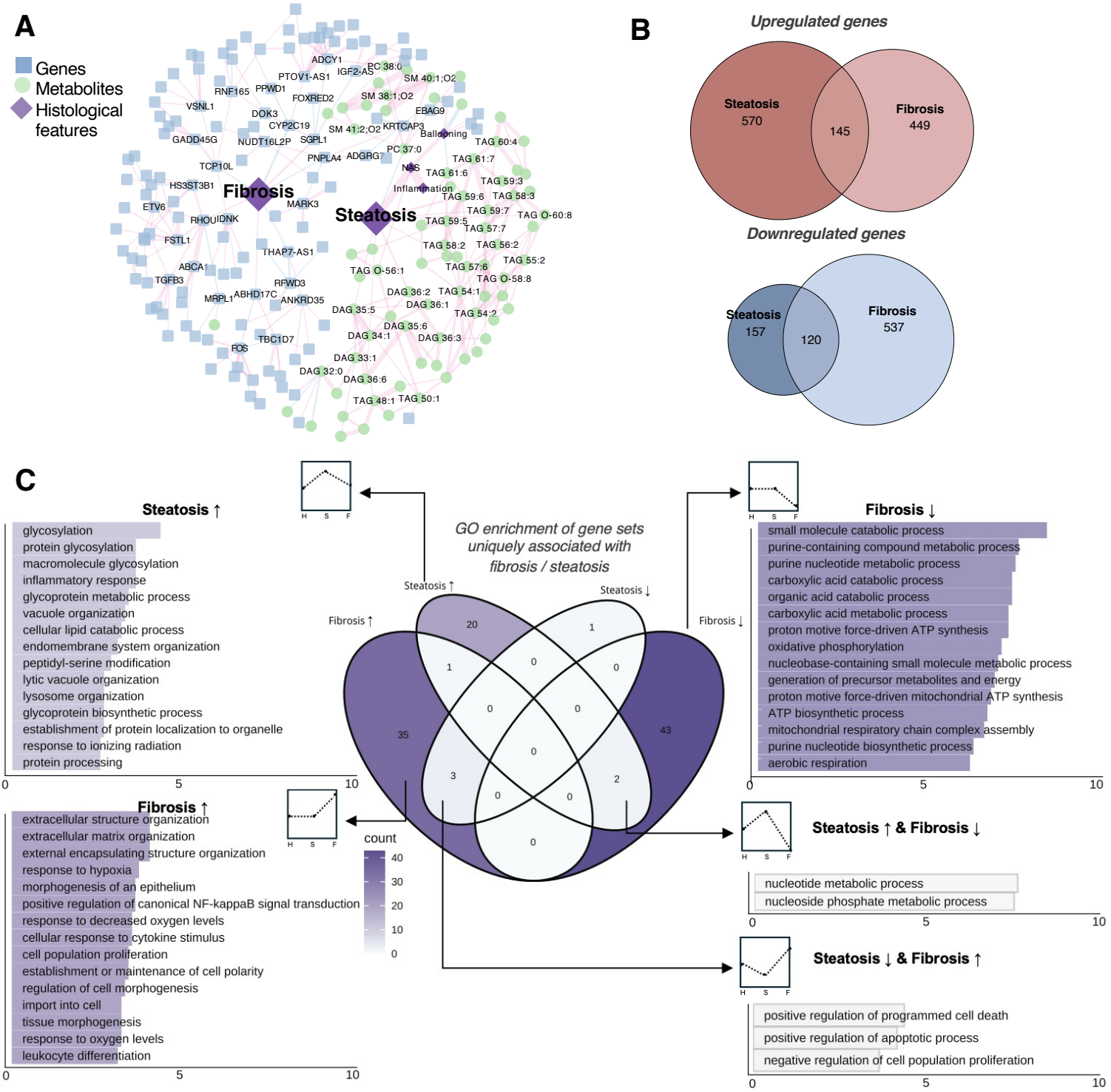

Figure 5. Steatosis and fibrosis as independent processes
(A) Network of genes, metabolites, and histological features (fibrosis and steatosis) using partial correlation analysis as described in the methods. (B) Venn diagrams depicting the number of genes significantly associated with steatosis and fibrosis (q value < 0.05). (C) Gene ontology (GO) enrichment of gene sets specific to steatosis or fibrosis. H, healthy obese controls. S, steatosis. F, fibrosis.

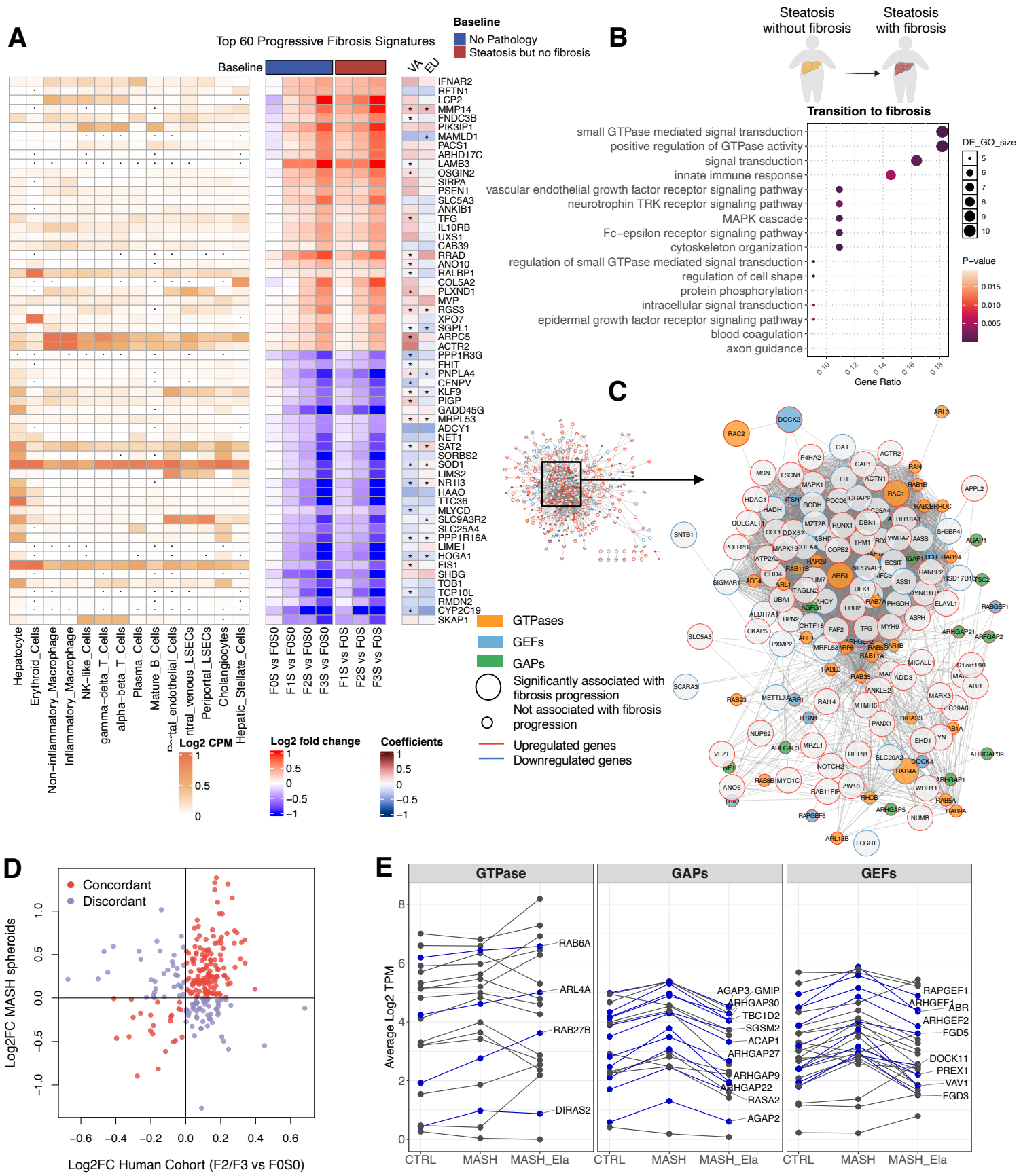

Figure 6. Liver fibrosis signatures and a potential therapeutic target of fibrosis initiation.
(A) Top 60 fibrosis markers in the liver. A total of 213 genes were identified, from which the top 30 upregulated and top 30 downregulated genes are visualized. The left side of the plot (blue bar on top) shows the comparison of individuals with fibrosis and individuals without pathology (baseline - "no MASLD"). For the right side (red bar), individuals with fibrosis were compared to those with steatosis but no fibrosis (baseline – "steatosis but no fibrosis"). Results were cross-referenced with two published cohorts (VA cohort, GSE130970; EU cohort, GSE135251, right). Asterisks indicate genes with a q-value < 0.05 and a consistent change in direction within our cohort. The average gene expressions of liver cell types were obtained from GSE115469 at the log2CPM level. Dots in the single cell map indicate zero expression in the corresponding cell types. (B) Enrichment of pathways in the transition from simple steatosis to the onset of fibrosis.

(C) Protein interaction network of GTPases and their regulators. Nodes are colored based on gene type, with borders indicating the direction of gene regulation. Node size corresponds to the significance of the genes in relation to fibrosis grades within this cohort. GEFs: Guanine nucleotide exchange factors. GAPs: GTPase-activating proteins. (D) Comparison of expression level changes in GTPase-related genes between this human cohort and an independent 3D spheroid MASH system. Log2 fold change for the human cohort was calculated by comparing patients with grade 2 or 3 fibrosis to those without fibrosis or steatosis. Genes with the same direction of change are colored in red, while others are colored in purple. (E) Expression of GTPase-related genes in patient-derived 3D liver spheroids (controls; MASH; MASH treated with Elafibranor; n = 4). Sixty-eight genes with a p-value < 0.05 from the ANOVA test were plotted in the diagram, with blue lines highlighting 24 genes that exhibited increased expression in the MASH group compared to the control group.